Fundamental Characteristics of Tropical Rain Cell Structures as Measured by TRMM PR

Yunfei FU[1*], Yilun CHEN[1], Xiangdong ZHANG[2], Yu WANG[1], Rui LI[1], Qi LIU[1], Lei ZHONG[1], Qiong ZHANG[3], and Aoqi ZHANG[1]

1 *School of Earth and Space Sciences, University of Science and Technology of China, Hefei* 230026, *China*
2 *International Arctic Research Center and Department of Atmospheric Sciences, University of Alaska Fairbanks, Fairbanks, AK* 99775, *USA*
3 *Department of Physical Geography and Bolin Center for Climate Research, Stockholm University, Stockholm* 10691, *Sweden*

(Received February 29, 2020; in final form June 14, 2020)

ABSTRACT

Rain cells are the most elementary unit of precipitation system in nature. In this study, fundamental geometric and physical characteristics of rain cells over tropical land and ocean areas are investigated by using 15-yr measurements of the Tropical Rainfall Measuring Mission (TRMM) Precipitation Radar (PR). The rain cells are identified with a minimum bounding rectangle (MBR) method. The results indicate that about 50% of rain cells occur at length of about 20 km and width of 15 km. The proportion of rain cells with length > 200 km and width > 100 km is less than 1%. There is a a log-linear relationship between the mean length and width of rain cells. Usually, for the same horizontal geometric parameters, rain cells tend to be square horizontally and lanky vertically over land, while vertically squatty over ocean. The rainfall intensity of rain cells varies from 0.4 to 10 mm h^{-1} over land to 0.4–8 mm h^{-1} over ocean. Statistical results indicate that the occurrence frequency of rain cells decreases as the areal fraction of convective precipitation in rain cells increases, while such frequency remains almost invariant when the areal fraction of stratiform precipitation varies from 10% to 80%. The relationship between physical and geometric parameters of rain cells shows that the mean rain rate of rain cells is more frequently associated with the increase of their area, with the increasing rate over land greater than that over ocean. The results also illustrate that heavy convective rain rate prefers to occur in larger rain cells over land while heavy stratiform rain rate tends to appear in larger rain cells over ocean. For the same size of rain cells, the areal fraction and the contribution of convective precipitation are about 10%–15% higher over land than over ocean.

Key words: rain cell, occurrence frequency, geometric parameters, physical parameters, Tropical Rainfall Measuring Mission (TRMM) Precipitation Radar (PR)

Citation: Fu, Y. F., Y. L. Chen, X. D. Zhang, et al., 2020: Fundamental characteristics of tropical rain cell structures as measured by TRMM PR. *J. Meteor. Res.*, **34**(6), 1129–1150, doi: 10.1007/s13351-020-0035-5.

1. Introduction

Precipitation systems are highly variable in geometric parameters (such as length, width, height, area, and horizontal and vertical shapes) and physical parameters (such as intensity, inhomogeneity, duration, rain type, and evolution stage of precipitation) under different synoptic situations (Austin and Houze, 1972; McAnelly and Cotton, 1989; Johnson et al., 2005; Turk and Bauer, 2006). They occasionally exhibit well-organized patterns, such as the spiral bands associated with tropical cyclones. However, they usually seem to display chaotic shapes, which are difficult to describe, in particular considering their spatial span across several orders of magnitude (Austin and Houze, 1972). To better represent precipitation systems and associated latent heat, or their parameterization in climate models, it is essential to accurately improve understanding of the geometric and physical characteristics of rain cells (Rossow et al., 2002; Arakawa, 2004; Pincus et al., 2006).

Supported by the National Natural Science Foundation of China (91837310 and 41675041), National Key R&D Program of China (2018YFC1507200 and 2017YFC1501402), Key Research and Development Projects in Anhui Province (201904a07020099), Third Tibetan Plateau Scientific Experiment: Observations for Boundary Layer and Troposphere (GYHY201406001), and Monitoring and Modelling Climate Change in Water, Energy and Carbon Cycles in the Pan-Third Pole Environment in the Framework of the European Space Agency and Ministry of Science and Technology of the People's Republic of China (ID：58516).

*Corresponding author: fyf@ustc.edu.cn.

Although rain cells are considered the most elementary unit of precipitation system in nature, there are different definitions of the rain "cell" in literatures. Austin and Houze (1972) analyzed the structure of precipitation patterns in New England, and found their dissimilarity. These precipitation patterns are fundamentally composed of sub-synoptic scale precipitation areas, each of which has clearly defined characteristics and behavior. Specifically, precipitation patterns can be recognized and described by four distinct scales of precipitation areas, including synoptic areas, large mesoscale areas, small mesoscale areas, and cells. The cell with an area about 10 km^2 is regarded as a single cumulus convective element in their study. At the beginning, a rain cell is usually regarded as a round precipitation area inside which the rain rate (or the radar reflectivity) is equal to or higher than a threshold rain rate or reflectivity (Sauvageot et al., 1999), and most studies investigated the relationship of area-averaged rain rate to the rain cell size distribution based on measurements from ground-based radar (Konrad, 1978; Gagin et al., 1986; Goldhirsh and Musiani, 1986; Capsoni et al., 1987; Bacchi et al., 1996; Sauvageot et al., 1999; Feral et al., 2000; Begum and Otung, 2009). Capsoni et al. (1987) defined rain cell as the area with rain rates (RR) greater than 5 mm h^{-1} observed by S-band radar near Milan during April–October 1980, and obtained a formulation for the spatial number density of rain cells to the cumulative RR distribution. This formulation was modified by Awaka (1989) with the threshold of RR at 0.4 mm h^{-1}.

To obtain the shape parameters, Feral et al. (2000) statistically studied rain cell geometric features by an ellipse-fitting approach to determine the length of major and minor axes including the orientation angle of rain cell. In determining horizontal dimensions of precipitation features, Nesbitt et al. (2006) also used the best-fit ellipse to locate rain cells and to obtain their major and minor axes. Subsequently, the distinct differences of storm morphology characteristics over land and ocean were found. Based on the best-fit ellipse approach, Liu and Zipser (2013) studied the morphology of convective precipitation systems over tropics and subtropics with more than 10-yr measurements of the Tropical Rainfall Measuring Mission (TRMM) Precipitation Radar (PR). They found that near-circular shaped areas of precipitation systems occurred more frequently over land while line areas showed higher frequency over ocean.

Although various methods have been employed to examine the features of rain cells measured by the TRMM PR, there are still some limitations in the definition of rain cell and errors due to swath truncation effect. In addition to those basic geometric parameters studied, more detailed parameters related to the shape and rain features are needed to investigate the three dimensional structure of rain cell. For example, the ellipse-fitting method may exclude some rainy areas of the target rain cell and result in an underestimate of rainfall amount. Meanwhile, the major and minor axes only represent the fitting ellipse morphology rather than that of the rain cell.

Furthermore, the measurements of PR inevitably suffer from swath truncation effect due to the limit of the TRMM swath width (215 km before boost and 245 km after boost). By analyzing a 3-yr TRMM PR dataset, Nesbitt et al. (2006) concluded that nearly 42% of total rainfall from precipitation systems is affected by swath truncation. Such an effect of swath truncation still existed in the statistical results obtained by Liu and Zipser (2013). Therefore, parameters described rain cell might be distorted because of the swath truncation that causes incompleteness of captured precipitation systems, especially for morphology parameters.

Additionally, studies aimed at analyzing the relationship between geometric features and RR in these rain cells need to further underline some important parameters, such as geometric shape parameters (horizontal and vertical morphology, i.e., spatial morphology) and physical parameters (fractions of different precipitation types, i.e., convective or stratiform), which may represent different stages of the precipitation system.

Based upon the above literature review, motivation of this study is to introduce an improved method for identifying rain cells and defining more detailed geometrical and physical parameters to describe three dimensional structure of rain cells. The paper is organized as below. Following the current section, a brief description of the datasets used in this study is presented in Section 2, together with the details of identification of rain cell and definition of associated parameters. The results are shown in Section 3, in which statistical characteristics of geometric and physical parameters for rain cells, the relationship among the geometric parameters, and the relationship between geometric parameters and physical parameters are displayed quantitatively. The spatial distribution characteristics of rain cells corresponding to several representative geometric and physical parameters are also given in this section. Section 4 provides conclusions of this study.

2. Data and methodology

In this study, the standard dataset of TRMM 2A25 at version 7 from January 1998 to December 2012 (https://

trmm.gsfc.nasa.gov/data_dir/data.html) was used. The 2A25 product derived from PR offers radar reflectivity profiles, precipitation profiles and type, such as convective and stratiform precipitation. The details about the TRMM algorithms may be found online at https://pmm.nasa.gov/resources/documents/TRMM. The PR works at 2.2-cm wavelength and scans across a swath 215 km (245 km after boost) wide with vertical and horizontal resolutions of 250 m and 4.3 km at nadir (5.0 km after boost), respectively. According to precipitation algorithms (Hitschfeld and Bordan, 1954; Kummerow et al., 1998, 2000; Iguchi et al., 2000; Schumacher and Houze, 2003; Awaka et al., 2009), briefly, a reflectivity profile is classified as "stratiform" if PR detects a bright band, i.e., a reflectivity maximum close to the freezing level about 5 km in altitude. If no bright band exists and any value of radar reflectivity in the beam exceeds a predetermined value of 39 dBZ, the profile is denoted as "convective." In this study, both stratiform (rain type marked by number 100–170) and convective (rain type marked by number 200–240) are our basic definition of "rain-type" contained in rain cells. The study of Liu and Fu (2001) showed that the amount of shallow precipitation is small except that over the southeast Pacific Ocean, so the present paper does not consider such a type of precipitation.

Because the TRMM PR operates at the Ku band (2.2-cm wavelength) with a sensitivity of approximately 17 dBZ (decreased to 18 dBZ after the boost in August 2001), it theoretically provides a better measurement for detecting the upper structures of precipitation systems including the echo top height than that by ground-based radar. In this study, the echo top height was detected by using the method by Liu et al. (2007). It is defined as the height of first layer from top to ground with a minimum radar echo exceeding 20 dBZ. It should be noted that the detection of echo top height is related to the wavelength of PR. The longer the wavelength of PR is, the lower the echo top height is detected.

According to PR scanning method within each across track covered by 49 pixels in the 215-km swath (245 km after boost), a rain cell is defined as rain pixels adjacent to each other with at least 0.4-mm h^{-1} near-surface rain rate or 17-dBZ reflectivity. Figure 1 shows the elementary categories of various connections among rain pixels. If given 4 rain pixels, there are 22 combination ways for their connections. It is obvious that the more connected rain pixels, the more arrangement ways for them, which forms diverse morphologies of rain cells. Considering that a rain cell has a certain size, we define a minimum size of rain cell by four connected rain pixels in PR measurement.

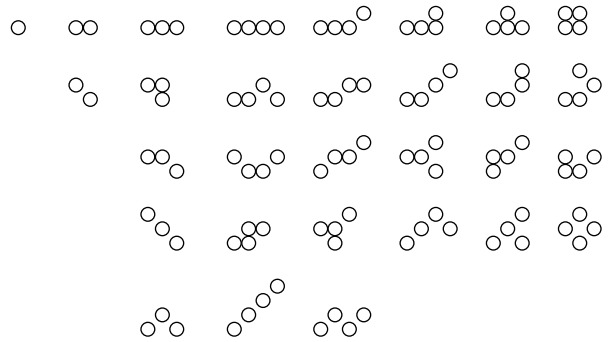

Fig. 1. The sketch diagram of elementary rain cells formed by different combinations of rain pixels measured by TRMM PR.

Another requirement of the definition is that rain cells identified within PR swath, which avoids the effect of swath truncation. Therefore, only complete rain cells within PR swath are included in this study. Then, a rain cell, at least four connected rain pixels, is defined as rain pixels by a minimum bounding rectangle (MBR). Based on the definition of the rain cell, a minimum length and width of the rain cell are near 10 and 5 km, respectively.

The MBR method used in this study, also called "bounding box" method, has been recorded as the International Standardization Organization (ISO) Number 19115 Metadata Standard for geospatial metadata. In its application, the employed "bounding box" needs to be rotated to fit the spatial distribution of targeted rain pixels to define rain cell. The length (L) of rain cell is the distance between the two ends of the targeted group of rain pixels along the direction that the "bounding box" has longer edges. Similarly, the width (W) of rain cell is defined along the other direction of the "bounding box." Both L and W are the horizontal dimensions of rain cell.

Figure 2 shows a schematic diagram of rain cell including convective (red) and stratiform (blue) rain pixels captured by the MBR method that can be relatively easily applied to search tens of thousands of rain cells in PR swathes. In the meantime, compared with the elliptical method, the MBR method would improve completeness of inclusion of rain pixels in the targeted rain cell, in particular for bow shaped rain cells or the small rain cells.

To describe the three dimensional geometric characteristics of rain cells, we designed series of parameters including the basic length (L), width (W), height (H_{avc} and H_{avs}), area (S), and series of shape parameters as shown in Table 1. The first five parameters in Table 1 are called the horizontal geometric parameters and the rest are the vertical geometrical parameters. Note that α (W/L) represents the two dimensional shape in the horizontal direction of rain cells. Small (large) α indicates that the

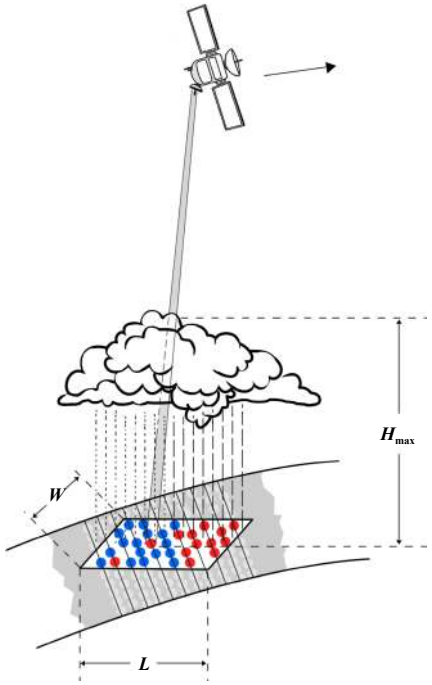

Fig. 2. The sketch of a rain cell containing pixels of convective (red) and stratiform (blue) rain captured by the MBR method.

Table 1. Definitions of geometric parameters of rain cell

Symbol	Geometric meaning
L (km)	Length of rain cell
W (km)	Width of rain cell
α	Horizontal shape of rain cell, $\alpha = W/L$
S (km^2)	Area of rain cell, sum of all areas of rain pixels
β	Filling ratio of rain cell, the ratio of rain cell area (S) to the fitted MBR area
H_{max} (km)	Maximum echo top height among rain pixels in the rain cell
H_{av} (km)	Mean echo top height averaged among rain pixels in the rain cell
γ_{max}	Maximum spatial morphology, $\gamma_{max} = H_{max}/L$
γ_{av}	Mean spatial morphology, $\gamma_{av} = 2H_{av}/(L + W)$
H_{avc} (km)	Mean echo top height of convective precipitation in the rain cell
H_{avs} (km)	Mean echo top height of stratiform precipitation in the rain cell

rain cell tends to have strip (square) shape and is more (less) likely related to precipitation of a frontal system. The variable β expresses the fraction of rain cell area (S) to the total MBR area (i.e., $L \cdot W$), which may provide information on the internal organization within the cell. Large (small) β indicates that those rain pixels are more (less) compactly organized and more (less) likely related to strong convective systems. The variables γ_{av} and γ_{max}, as the parameters of rain cell spatial morphology, represent the three dimensional shape, i.e., the ratio of its vertical extension to its horizontal size. Small γ_{av} (γ_{max}) means a "squatty" appearance of rain cell compared to "lanky" appearance for large γ_{av} (γ_{max}). This set of parameters provides a three dimensional view of the complex rain cell structure.

After determining the geometric parameters of rain cell, the physical parameters of rain cell are defined as well. Based on rain types, rain rate profiles and near surface RR supplied at version-7 2A25, those physical parameters of rain cell (Table 2) include mean rain rate (RR_{av}), mean convective/stratiform rain rate (RR_{avc}/RR_{avs}), the maximum rain rate (RR_{max}), the maximum rain rate of convective/stratiform precipitation (RR_{maxc}/RR_{maxs}), convective/stratiform area fraction (CAF/SAF, the ratio of convective/stratiform areas to total precipitation areas within rain cell), and convective/stratiform precipitation contribution (CPC/SPC, the ratio of convective/stratiform precipitation to total precipitation within rain cell). Those parameters are important to represent the intensity, the inhomogeneity, and the evolution stage of rain cells.

As an example, Fig. 3 shows two rain cells captured by the MBR method. Near surface rain rate and rain types (stratiform, shallow, and convective) within the two cells were measured by PR along the equator of western Pacific on 31 March 1998, and in the Indian Peninsula on 26 May 1998, respectively. Table 3 shows the calculated geometric and physical parameters of the two rain cells displayed in Fig. 3.

The first case is a mesoscale rain cell with L = 212.32 km, W = 67.11 km, S = 4400 km^2, and H_{av} = 5.97 km, which shows a strip like shape (α = 0.316) as measured by PR. This rain cell has parameters of γ_{av} = 0.043 and γ_{max} = 0.054, showing the vertical scale at least an order smaller than horizontal scale. The physical parameters of

Table 2. Definitions of physical parameters of rain cell

Symbol	Physical meaning
RR_{av} (mm h^{-1})	Mean rain rate obtained by averaging all rain rates within the rain cell
RR_{max} (mm h^{-1})	Maximum rain rate among rain pixels of the rain cell
RR_{avc} (mm h^{-1})	Mean convective rain rate averaged by all convective rain rates within the rain cell
RR_{avs} (mm h^{-1})	Mean stratiform rain rate averaged by all stratiform rain rate within rain cell
RR_{maxc} (mm h^{-1})	Maximum rain rate among convective pixels of the rain cell
RR_{maxs} (mm h^{-1})	Maximum rain rate among stratiform pixels of the rain cell
CAF (%)	Fraction of convective area to total precipitation area within the rain cell
SAF (%)	Fraction of stratiform area to total precipitation area within the rain cell
CPC (%)	Convective precipitation contribution to total precipitation within the rain cell
SPC (%)	Stratiform precipitation contribution to total precipitation within the rain cell

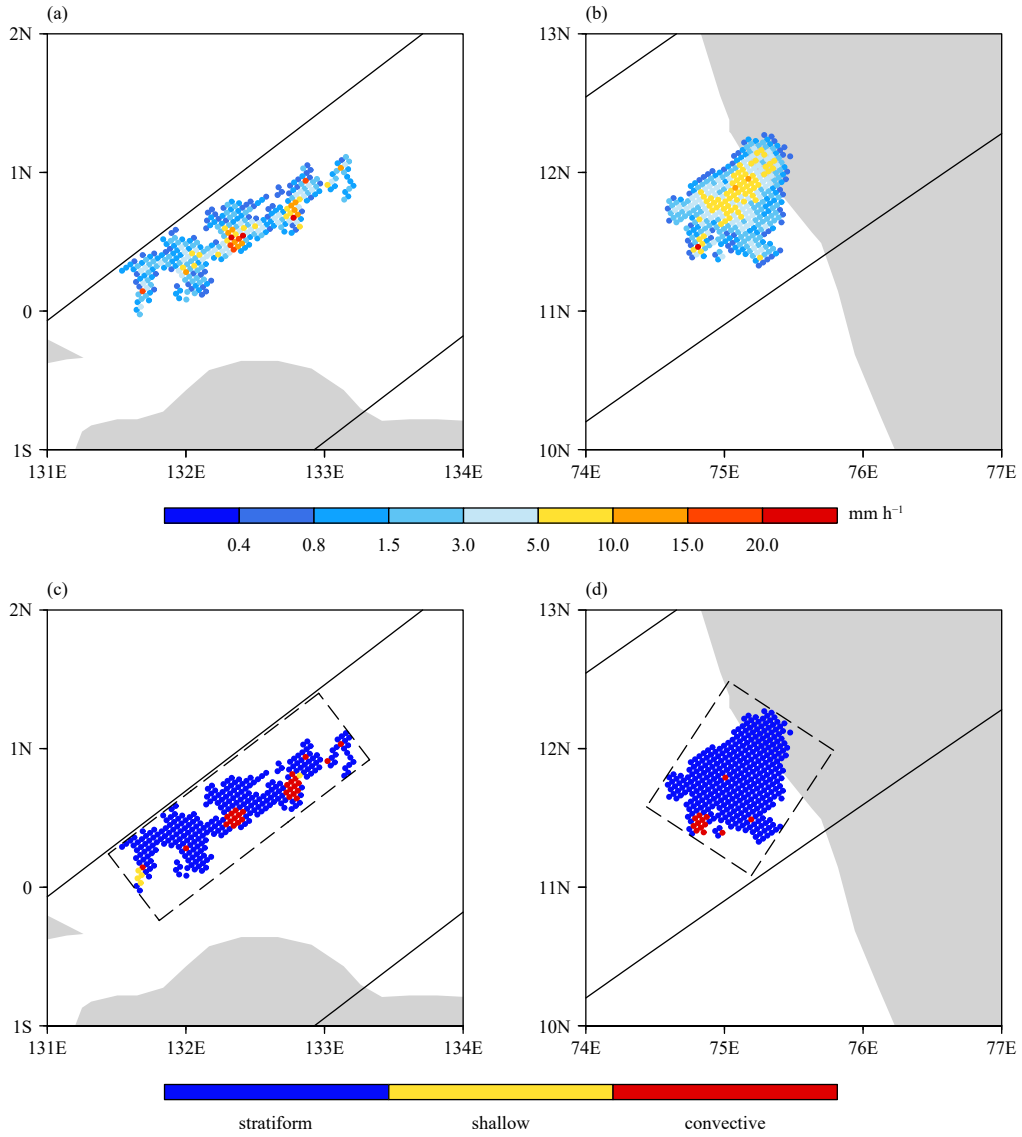

Fig. 3. Near surface rain rate of two rain cells that occurred in (a) the equator of western Pacific on 31 March 1998 and (b) Indian Peninsula on 26 May 1998 measured by PR. In (c, d), rain pixels with blue, yellow, and red represent stratiform, shallow, and convective precipitation, respectively, captured by the MBR for both rain cells. The shaded (unshaded) background represents the land (ocean).

CAF = 9.24% and SAF = 89.11% indicate dominated area of stratiform precipitation in this rain cell. This rain cell has RR_{av} = 2.84 and RR_{max} = 27.75 mm h^{-1}, respectively, and its RR_{avc} and RR_{avs} show 12.1 and 1.88 mm h^{-1}, respectively.

For the second case (Fig. 3b), L, W, S, and H_{av} are 119.54 km, 99.13 km, 5140 km^2, and 9.36 km, respectively. The rain cell shows a quasi-square shape with larger parameter α = 0.829, much larger than that in the first case (α = 0.316). The parameters γ_{av} = 0.096 and γ_{max} = 0.094 are slightly larger than both in the first case, which means that the second rain cell is slightly taller than the first case. Generally, the above indicates the relative square horizontal shape with slightly tall in the second rain cell compared with long strip shape with low in the first rain cell. The parameters RR_{av} and RR_{max} are 3.17 and 23.05 mm h^{-1} at this rain cell associated with RR_{avc} = 5.86 mm h^{-1} and RR_{avs} = 3.07 mm h^{-1}, respectively, which are comparable to those in the first case. In addition, CAF (SAF) in the second case has a value of 3.67% (96.32%), smaller (larger) than that in the first case. This indicates that the rain cell in the first case has larger proportion of the area with convective precipitation (9.24%), while the second rain cell has larger proportion of the area with stratiform precipitation (96.32%). Relatively, the quasi-square rain cell in the second case is more compacted than the strip-like rain cell in the first case, as quantitatively described by β (0.309 vs. 0.434).

Table 3. The calculated geometrical (horizontal and vertical) and physical parameters of the first/second case

Horizontal parameter		Vertical parameter		Physical parameter	
L (km)	212.32/119.54	H_{max} (km)	11.50/11.50	RR_{ave} (mm h^{-1})	2.84/3.17
W (km)	67.11/99.13	H_{av} (km)	5.97/9.36	RR_{max} (mm h^{-1})	27.75/23.05
α	0.316/0.829	γ_{max}	0.054/0.096	RR_{avc} (mm h^{-1})	12.1/5.86
S (km^2)	4400.2/5140.8	γ_{av}	0.043/0.094	RR_{avs} (mm h^{-1})	1.88/3.07
β	0.309/0.434	H_{avc} (km)	6.73/9.25	CAF (%)	9.24/3.67
		H_{avs} (km)	5.93/9.37	SAF (%)	89.11/96.32

Generally, these two cases show two different types of rain cells featured by distinct geometric and physical parameters, and they are all well described by our method. In the study, we totally capture more than 14,436,000 rain cells by the MBR method over the tropics (2,429,116 cells over land and 12,007,529 cells over ocean) in the belt of 20°S–20°N during 15 yr from 1998 to 2012.

3. Results and discussion

3.1 *Statistical characteristics of geometric and physical parameters*

Based on the definition of the geometric and physical parameters of rain cell, we firstly analyze their statistical characteristics to understand their nature. The result indicates that the probability distribution functions (PDFs; Fig. 4) of L reach the peak of 50% when L is at 20 km, i.e., the occurrence frequency of rain cell (OFRC) with 20 km in length is 50%. The OFRC decreases with the increase of L when L is greater than 20 km no matter over land or ocean (Fig. 4a). When L is longer than 200 km, the OFRC decreases rapidly lower than 1%. When L is less than 20 km, the OFRC increases with the increase of L. Similarly, the PDF of W reaches the peak of 50% when W is 15 km (Fig. 4b). Meanwhile, the OFRC of large W is very low (less than 1%), when W is larger than 100 km. This suggests that few rain cells are greater than 100 km in width. Comparison of the PDF distributions of both L and W indicates that about 50% of rain cells occur at dimensions of 20 km in length and 15 km in width. Note that the width of rain cell in reality may be wider than 220 km (the width of PR swath). However, as shown in Fig. 4b, the OFRC with W greater than 100 km

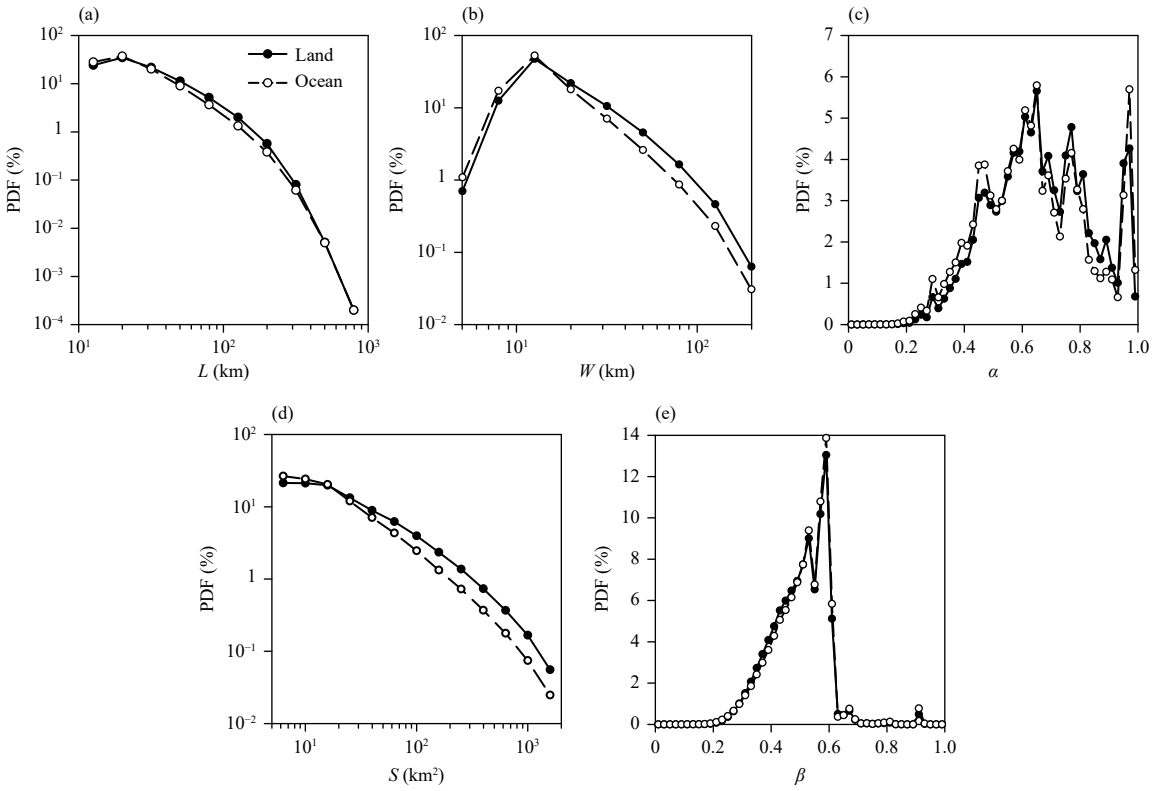

Fig. 4. Probability distribution functions (PDFs) of the horizontal geometrical parameters: (a) L, (b) W, (c) α, (d) S, and (e) β, over tropical land and ocean calculated from 1998 to 2012.

is less than 1%. It is therefore that possible discrepancies between the rain cells detected in this study and those in the real world should not cause noticeable biases and then influence the conclusions from this study. Statistics in Table 4 show that the mean length of rain cells is 30.25 and 27.11 km over land and ocean, respectively, 18.75 and 15.97 km at the mean width, respectively.

The PDF of the parameter describing horizontal shape of rain cell, α, is displayed in Fig. 4c. It shows that both curves represented for land and ocean have almost the same feature, which indicates very low OFRC (less than 10%) for "long strip" shape ($\alpha < 0.4$) and for "square" shape ($\alpha > 0.8$). The rest rain cells are featured between the two shapes. Generally, the mean α of rain cells is 0.66 (0.64) over land (ocean) as shown in Table 4, i.e., most rain cells prefer to exhibit long strip shape other than square shape in their mean state.

In terms of the horizontal "size," the OFRC decreases with increase of rain cell area S (Fig. 4d). When S is greater than 1000 km^2, the OFRC only has about 5%. For S larger than 400 km^2, the OFRC over land is higher than that over ocean for the same rain cell area, which is consistent with the previous study (Nesbitt et al., 2006). Statistical calculation in Table 4 indicates that the mean rain cell area S is 368.5 (264.5) km^2 over land (ocean). The PDF of β mainly varies between 0.25 and 0.6 with peak nearly at 0.6. The PDF pattern of β shows almost half rain cells with β greater than 0.5. Actually, the mean β in Table 4 is 0.50 (0.51) over land (ocean). These rain cells are nearly filling more than half area of the fitting MBR, which illustrates the effectivity of the MBR method on capturing rain cells in this study.

The PDFs of vertical geometrical parameters of rain cells over tropical land and ocean calculated from 1998 to 2012 are plotted in Fig. 5. In contrast to the similarity of horizontal parameters of rain cells over land and ocean as shown in Fig. 4, remarkable difference of PDFs of vertical parameters between them is found in Fig. 5. It shows that the PDF of H_{max} gets its single peak at 6 km over land, but double peaks at 3 and 6 km over ocean. The PDF peak of H_{max} at 3 km over ocean should correspond to warm rain cells, i.e., shallow isolated precipitation (Schumacher and Houze, 2003; Qin and Fu, 2016), while the peak at 6 km over land and ocean is related to deep rain cells whose storm top height are above the freezing layer (about 4.5 km in tropics, usually; Shen et al., 2000). Figure 5a also shows that the PDF of deep rain cells ($H_{max} > 6$ km) over land is larger than that over ocean, which is due to the intense thermal forcing of land surface (Benjamin and Carlson, 1986). The mean H_{max} is 7.34 (5.44) km over land (ocean) in Table 4. Subsequently, the above features are shown in Fig. 5b for the PDF of H_{av}. It indicates that H_{av} varies from 2 to 10 km with peak at 5 km over land, and 2 to 7.5 km with peak at 3 km over ocean. Statistical calculations in Table 4 indicate that the mean H_{avc} and H_{avs} are 6.54 and 5.41 km over land, respectively, 5.67 and 4.71 km over ocean, respectively. Briefly, the above hints that shallow warm rain cells are the common precipitation system while deep rain cells are relative less over ocean than that over land.

As parameters reflecting spatial morphology of rain cell, i.e., "squatty" or "lanky" appearance, both γ_{max} and γ_{av} mainly vary from 0.05 to 0.65 over land and ocean, and both of them get peak at ~0.2 over ocean and ~0.25 over land as shown in Figs. 5c, d. The mean γ_{max} and γ_{av} are 0.31 and 0.29 over land, 0.25 and 0.23 over ocean (Table 4). Generally, the PDFs of both γ_{max} and γ_{av} are narrower over ocean than those over land. The PDF patterns in Figs. 5c, d illustrate higher OFRC in lanky appearance over land while more squatty appearance over ocean. It is clear that the parameters of γ_{max} and γ_{av} display directly the spatial morphology of rain cells, which is helpful to comparison of rain cells by their appearances.

The physical parameters of rain cells describe various aspects of physical properties of precipitation systems, such as rainfall intensity of different types of precipitation systems. According to the definition mentioned in Section 2, these parameters are the mean surface rain rate (RR_{av}), the maximum surface rain rate (RR_{max}) of rain cell. RR_{av} and RR_{max} are also further calculated for convective and stratiform precipitation, respectively, within each rain cell, represented by RR_{avc}, RR_{avs}, RR_{maxc}, and RR_{maxs}, respectively. Considering the differences in

Table 4. The calculated mean geometrical (horizontal and vertical) and physical parameters of rain cells over land/ocean. Samples of rain cells are 2,429,116 over land and 12,007,529 over ocean, respectively

Mean horizontal parameter	Land/ocean	Mean vertical parameter	Land/ocean	Mean physical parameter	Land/ocean
L (km)	30.25/27.11	H_{max} (km)	7.34/5.44	RR_{av} (mm h^{-1})	2.92/2.52
W (km)	18.75/15.97	H_{av} (km)	5.45/3.94	RR_{max} (mm h^{-1})	11.59/8.16
α	0.66/0.64	γ_{max}	0.31/0.25	RR_{avc} (mm h^{-1})	6.84/6.80
S (km^2)	368.5/264.5	γ_{av}	0.29/0.23	RR_{avs} (mm h^{-1})	1.51/1.63
β	0.50/0.51	H_{avc} (km)	6.54/5.67	CAF (%)	26.6/13.4
		H_{avs} (km)	5.41/4.71	SAF (%)	56.5/34.5

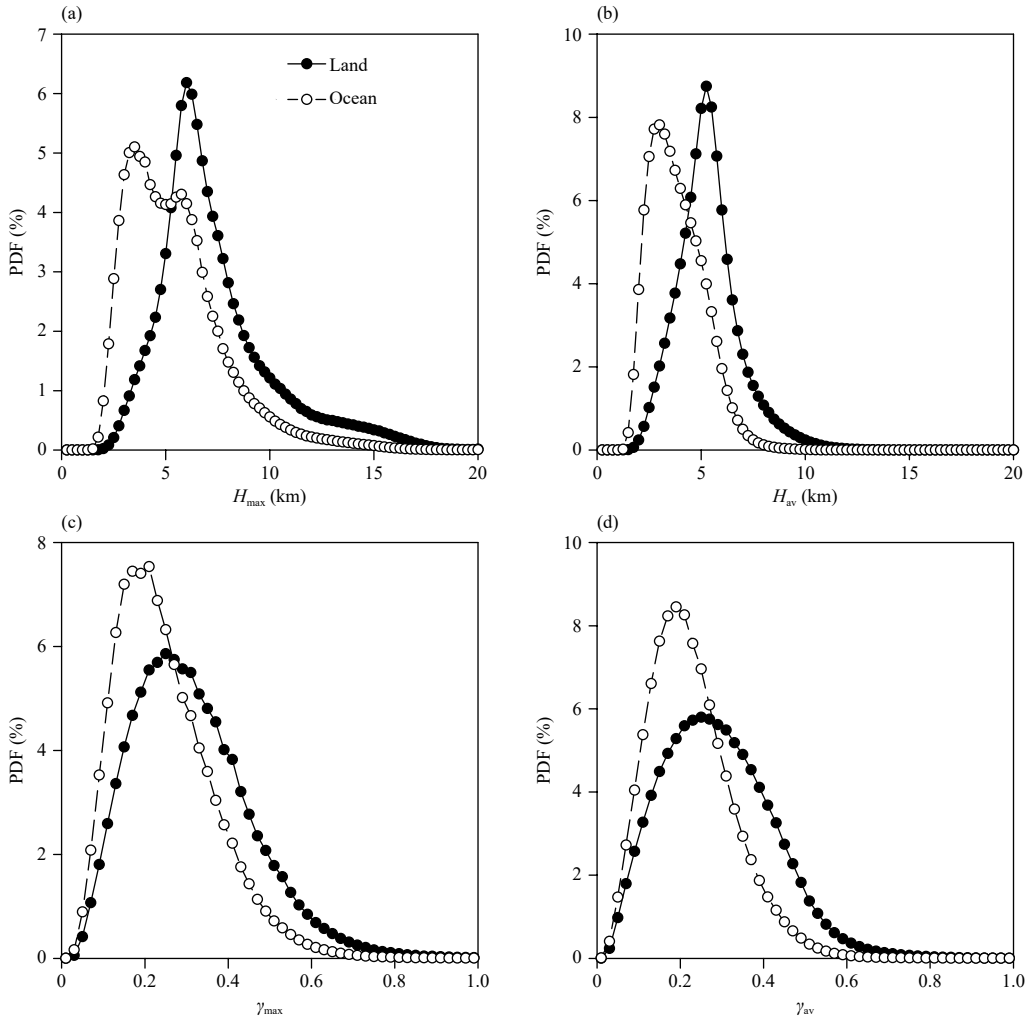

Fig. 5. As in Fig. 4, but for (a) H_{max}, (b) H_{av}, (c) γ_{max}, and (d) γ_{av}.

covered area and intensity of convective and stratiform precipitation within rain cells, CAF, SAF, CPC, and SPC are also defined in Table 2.

Figure 6 shows the PDFs of these physical parameters over tropical land and ocean. It indicates that RR_{av} varies from 0.4 to 10 mm h^{-1}, peaking at ~1 mm h^{-1}, for rain cells over land, and from 0.4 to 8 mm h^{-1}, peaking at 2–2.5 mm h^{-1}, over ocean (Fig. 6a). Table 4 shows RR_{av} = 2.92 (2.52 mm h^{-1}) over land (ocean). RR_{av} appears to have a broader distribution associated with rain cells over land than that over ocean. The PDFs of heavy rain (RR_{av} > 4 mm h^{-1}) and light rain (RR_{av} < 1.5 mm h^{-1}) are higher over land than those over ocean. Over ocean, about 80% rain cells have RR_{av} from 1.5 to 4 mm h^{-1}. The PDF of RR_{max} is similar to that of RR_{av}. The mean RR_{max} in Table 4 is 11.59 mm h^{-1} and 8.16 mm h^{-1} over land and ocean, respectively. It should be note that the higher PDF of light RR over land could be associated with air pollution emitted by human activities and/or mineral dust, which has been reported by studies (Rosenfeld et al., 2008; Halfon et al., 2009; Fu et al., 2016; Li and Min, 2010; Li et al., 2010). It needs to be investigated whether rain cells with light rain rate over land are located in higher aerosol emission regions.

The PDFs of RR_{avc}, RR_{maxc}, RR_{avs}, and RR_{maxs} are plotted in Figs. 6c–f for rain cells over land and ocean. They show small difference between land and ocean. However, the difference between convective and stratiform precipitation is clear, showing wider range of RR_{avc} and RR_{maxc}, peak at ~6 mm h^{-1}, than that of RR_{avs} and RR_{maxs}, peak at ~1.5 mm h^{-1}. In Table 4, statistical results indicate that the mean RR_{avc} and RR_{avs} are 6.84 (6.80 mm h^{-1}) and 1.51 (1.63 mm h^{-1}) over land (ocean), which are different from the results derived from the statistics of PR pixel-level data. In tropical and subtropical regions, statistics of RR shows the convective RR ranging from 2 to 18 mm h^{-1} with peak at ~8 mm h^{-1}, while the stratiform RR varying from 0.5 to 4.5 mm h^{-1} with

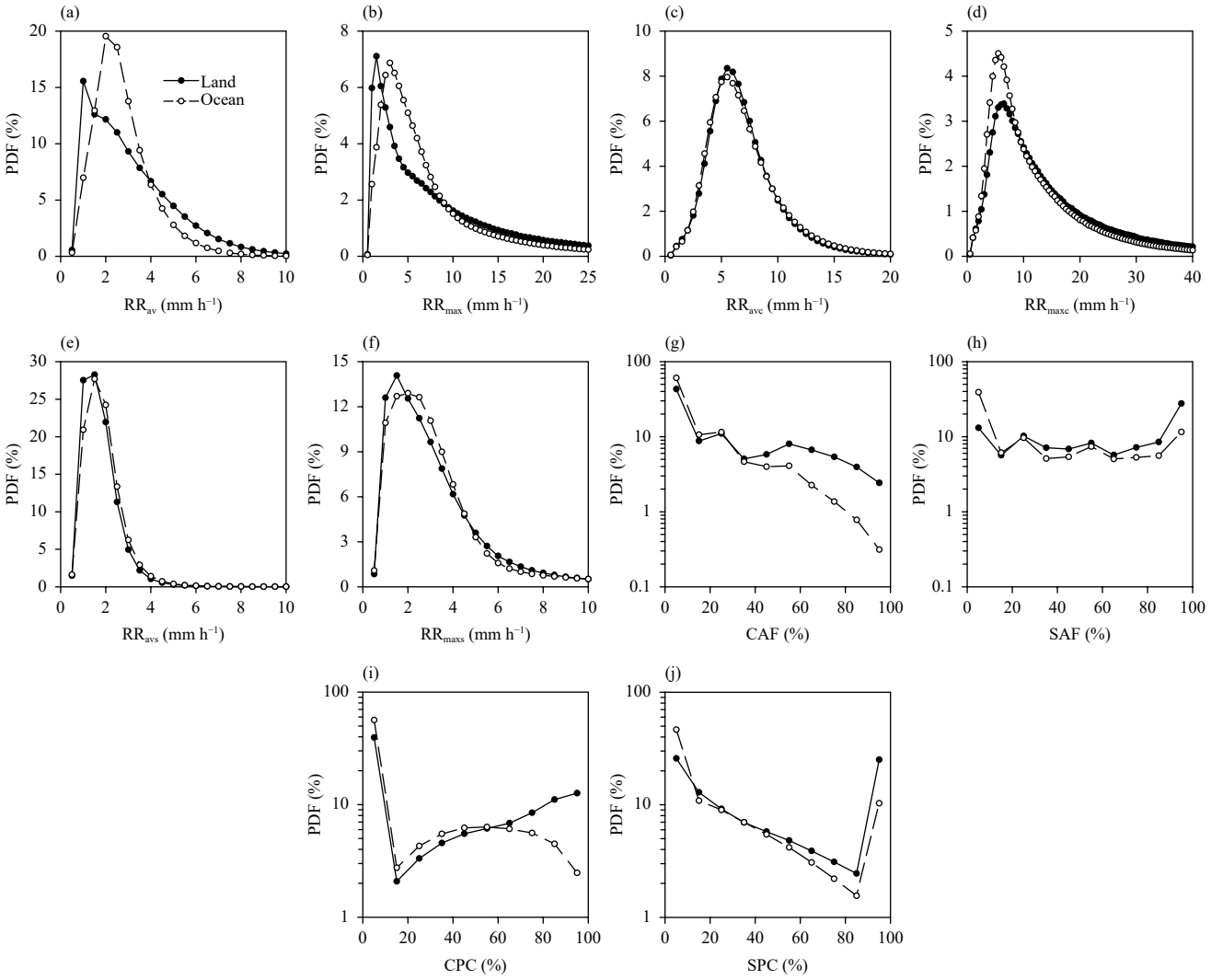

Fig. 6. As in Fig. 4, but for (a) RR_{av}, (b) RR_{max}, (c) RR_{avc}, (d) RR_{maxc}, (e) RR_{avs}, (f) RR_{maxs}, (g) CAF, (h) SAF, (i) CPC, and (j) SPC.

peak at 2 mm h^{-1} (Liu et al., 2013). Therefore, statistically, the peak RR_{avc} (RR_{avs}) is slightly smaller than that of RR for convective (stratiform) precipitation at PR pixel level, because RR_{avc} (RR_{avs}) is an arithmetic average RR among all rain pixels within rain cells.

The area fraction covered by convective precipitation or stratifrom precipitation in rain cell, defined by CAF or SAF, also reflects precipitation natures to a certain extent, for example, whether rain cell tends to be convective or stratiform. These natures may link to the developing stage of rain cell (Schumacher and Houze, 2003). Previous studies by using PR pixel-level data indicated that CAF and SAF were nearly 12% and 80%, respectively, in the tropics and subtropics (Liu and Fu, 2001). Table 4 shows that mean CAF and SAF of rain cell are 26.61% (13.40%) and 56.51% (34.48%) over land (ocean), which represents that CAF over land is near two times higher than that over ocean, and higher SAF over land than that over ocean. The later possible is because there are many shallow rain cells over ocean in our statistical calculation.

The PDFs of CAF and SAF shown in Figs. 6g, h indicates that the PDF decreases sharply with the increase of CAF within rain cells. For example, 30% (50%) rain cells have CAF less than 10% over land (ocean). For rain cells having 80% CAF, there are only less than 4% PDF over land and 1% over ocean, which indicates more rain cells with higher CAF over land than over ocean. This should be the result of much more atmospheric instability over land, which easily leads to much more convective activities. In contrast, the difference of SAF over land and ocean is not obvious when SAF varies from 15% to 9%. However, when SAF is larger (less) than 90% (15%), rain cells over land are more abundant (less) than those over ocean. For example, there exists 27.5% and 11.5% rain cells over land and ocean, respectively, when

their SAF is the same, at 90%. Physically, there should be more rain cells being dominant stratiform precipitation over ocean than over land. But in this study, a large number of rain cells mixing with shallow precipitation over ocean result in the small ratio of stratiform area to the total rain area. Follow-up studies in definition of rain cell separating out rain cells of shallow precipitation will be carried out in details.

As previous statistical studies pointed out, the contribution of both convective and stratiform precipitation to the total precipitation is almost equal over the tropics and subtropics because the intensity of convective precipitation is large although its proportion of spatial coverage is small compared with stratiform precipitation (Liu and Fu, 2001; Schumacher and Houze, 2003; Liu et al., 2013). If we consider these two types of precipitation elements within a rain cell, what are their relative contributions to total precipitation? Figure 6i shows that the PDF of CPC decreased sharply from about 40% (50%) to 2% (2.5%) as the CPC increased to 15%, and then it abidingly increases 2% (2.5%) to 10% (6%) as CPC varies from 15% to near 100% (55%) over land (ocean). The CPC at 15% is the valley point of the PDF (~2% and 2.5%) for both over land and ocean. The PDF decreases from 6% to 2% when CPC increases from 55% to near 100% over ocean. This indicates that convective precipitation in most rain cells contributes less than 15% to the total precipitation over land and ocean, while there are much more rain cells over land having CPC over 60% than those over ocean. Similarly, Fig. 6j shows that the PDF also decreases from 25% (50%) to less than 2.5% (1.5%) as SPC increases to 85% over land (ocean), and then it sharply increases to 30% (10%) as SPC varies from 85% to near 100% over land (ocean). We speculate that the abnormal high PDFs with large SPC or CPC are related to some special synoptic systems.

The above PDF analysis suggests that the MBR method captures half of rain cells having 20 km in length and 15 km in width. The proportion of rain cells with L longer than 200 km and width wider than 100 km is less than 1%. There is a higher proportion of rain cells with area larger than 400 km^2 over land than over ocean. Relatively, most rain cells exhibit horizontal long strips over land. Vertically, most rain cells over land are higher than those over ocean, nearly 1 km higher on average. Therefore, these rain cells over land look with lanky appearance compared with rain cells with squatty appearance over ocean. The PDF of the physical parameters indicates that the variation range of rainfall intensity over land is larger than that over ocean, but convective precipitation intensity shows no such a difference. When the CAF is more than 50%, or when the CPC to the total precipitation is more than 60%, within a rain cell, such a kind of rain cells easily occur over land.

3.2 *The relationship among the geometric parameters*

It is important to know the relationship among the geometric parameters of rain cells because the linkages of these parameters reflect the nature of rain cells, which may supply the acquired knowledge for weather models to make optimal simulations. Previous knowledge has shown that the cumulonimbus cloud is high in the vertical direction while the nimbostratus cloud generally distributes broadly in the horizontal direction (Houze, 1981; Houze and Betts, 1981). Although observations of ground-based or ship-based weather radar have been operated for many years or curried out in a limited number of experiments (Dixon and Wiener, 1993; Short et al., 1997), the relationship between the horizontal geometric parameters and the vertical scale of rain cells over land and ocean is still unclear because the statistical results were short of large samples.

However, the obtained geometric parameters of rain cells with about 14,436,000 samples in this study make it reliable to reveal the relationship among these parameters including the horizontal and vertical scales. Considering the reliability of statistical results in our calculations, the approach of equal sample statistics is adopted. This approach has been used to calculate the mean and standard deviation of rain rate variation with altitude (Fu et al., 2018). Specifically in this study, an independent variable (x axis) is divided into 40 intervals, i.e., 2.5% of the total samples in each interval, and then the values of a dependent variable (y axis) are averaged within each interval. Correspondingly, standard deviations are also calculated within each interval.

First, the relationship between L (x axis) and W (y axis) is shown in logarithmic coordinates in Fig. 7. It displays that L has a log-linear relationship with W when L is longer than 20 km for rain cells over land and ocean, which can be described by the equation, $\log W = a + b \times \log L$. Here, $a = -0.0938$, $b = 0.9193$ over land, and $a = -0.0701$, $b = 0.881$ over ocean. Such relationship between L and W physically means the horizontal shape of rain cell that maintains its ratio between L and W during its growing process. As suggested by Liu and Zipser (2013), line shapes of rain cells are mostly formed under a particular condition, such as in a complex area or influenced by some weather systems. The logarithmic linear relationship between L and W of rain cell may be the universal feature for precipitation systems in tropics. When L is less than ~20 km (W < ~15 km), i.e., small rain cells,

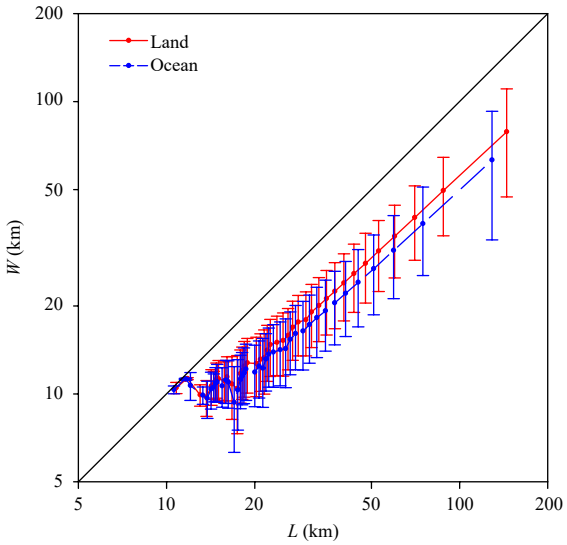

Fig. 7. The relationship between W and L over tropical land and ocean from 1998 to 2012 based on the statistical principle of same samples in each interval at x axis.

the relationship between the both parameters seems complex. For these rain cells, both parameters are greatly influenced by a variety of combinations of rain pixel locations geometrically, which may suggest that the horizontal geometric parameters change strongly at the beginning process of rain cells physically.

In order to better understand the horizontal structure of rain cells, the relationship between the horizontal morphological parameters (α and β) and the horizontal geometric parameters (L, W, and S) are analyzed as shown in Fig. 8. Figure 8a displays that the parameter α decreases from 1.0 (square rain cell) to about 0.6 (quasi-square rain cell) rapidly with the increase of L from 10 to 20 km. When L continuously increases from 20 to about 200 km, α decreases slowly from 0.6 to about 0.5 (relative long rain cell). This confirms the feature of ratio change between L and W as shown in Fig. 7, i.e., they generally follow a logarithmic linear relation. To keep such ratio change, in Fig. 8b, the parameter α varies less as W is greater than ~15 km. When W is less than ~15 km, α increases from 0.4 (long rain cell) to 0.65 (quasi-square rain cell) with the increase of W. However, as mentioned above, the PR swath is about 215 km (245 km after boost) so that the extremely-large rain cells will be cut off by the orbital edge; fortunately, there are not many of such kind of rain cells as displayed in Fig. 4a, so that our statistical results will not be seriously affected.

The ratio change between L and W also determines that the parameter α (W/L) decreases with the increase of

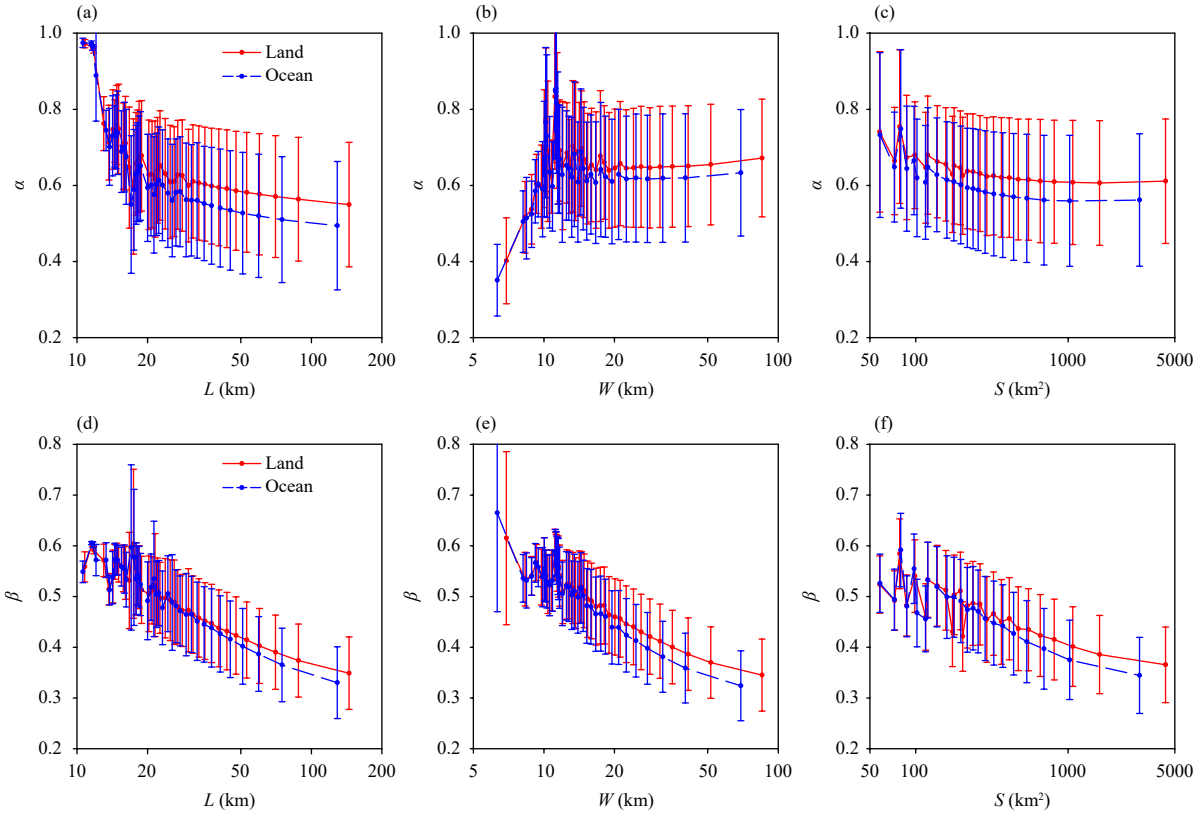

Fig. 8. Relationships between (a) α and L, (b) α and W, (c) α and S, (d) β and L, (e) β and W, and (f) β and S over tropical land and ocean from 1998 to 2012 based on the statistical principle of same samples in each interval at x axis.

rain cell area S over land and ocean when S is less than 300 km^2 (less than ~20 pixels), which means that the shape of rain cells easily changes from square shape to relatively line strip shape when their areas increase to 300 km^2. As S is larger than 300 km^2, α is nearly constant (Fig. 8c), which still means the ratio changes for rain cells. The above indicates that α combining the length and width of rain cell is also a parameter describing the horizontal shape of rain cells. It is noted that for the same horizontal geometric parameters of rain cells, i.e., the same L, W, and S, α over land is greater than that over ocean, i.e., more likely to be square shape for rain cells over land, which agrees with the results obtained by using the ellipse-fitting method (Liu and Zipser, 2013).

The parameter β, ratio of S to the area of the fitting MBR, decreases in the condition of $L >$ ~20 km, $W >$ ~15 km, or $S >$ 300 km^2 with the increase of L, W and S, respectively, as shown in Figs. 8d–f. This expresses the incompact horizontal structure of rain cells over land and ocean when their horizontal geometric parameters get increase, such as rain cells in their mature process. Generally, for given horizontal geometric parameter (L, W, or S), the horizontal structure of rain cells is more compact over land than over ocean. For rain cells with small horizontal geometric parameters ($L <$ ~20 km, $W <$ ~15 km, or $S <$ 300 km^2), β of these cells varies around 0.5 or above 0.5, which indicates the relatively compact distribution of these cells.

The storm-top height (STH) can be measured directly by TRMM PR (Fu et al., 2012; Chen et al., 2016), which is different from the spectrum method using an infrared retrieval algorithm (Lau and Wu, 2011). Usually, STH is related to the developing stage of precipitation systems. Statistics show that the intensity of surface RR varies with STH at the quadratic functions in the tropics (Fu et al., 2012; Chen et al., 2016). Liu and Zipser (2013) gave the two dimensional histogram of rain cells as the function of their area and the maximum height of 30 dBZ. They found that except shallow precipitation, large rain cells are usually associated with higher cloud top and greater echo intensity than those of small rain cells. Chen et al. (2017) obtained the relationship among the cloud-top height, the maximum reflectivity, and the cross-section area of cloud clusters by using the Cloud Profiling Radar carried by CloudSat. However, in both studies, only the maximum value, such as H_{max} or RR_{max}, among all samples, is chosen to represent the rainfall intensity of rain cells.

To reveal the relationship between the vertical extension parameters, both the maximum and the average STH (H_{max} and H_{av}), and the horizontal geometric parameters (L, W, and S) for rain cells over land and ocean are studied. Figure 9 shows the statistical results that H_{max} and H_{av} consistently increase with the increase of the horizontal geometric parameters over land and ocean. The increasing slope of H_{max} shows greater than that of H_{av}, i.e., H_{max} increases faster with horizontal geometric parameters, whereas the variation of H_{av} with S seems following a nearly logarithmic linear rate over land and ocean. The variance of H_{av} is also slightly smaller than that of H_{max}. This result suggests that H_{av} may effectively express the relationship between extension and horizontal scale of rain cells because it filters out the errors caused by random or extreme values. Figure 9 also shows that in the case of rain cells with a same horizontal geometric parameter (L, W, and S), H_{max} and H_{av} over land are about 1.5 km higher than that over ocean, i.e., rain cells are deeper over land than over ocean for the same horizontal geometric parameter, which may suggest different effects of surface forcing by land and ocean on rain cells. This would be useful information for evaluating model simulations in rain cells.

The relationship between spatial morphology (γ_{max} and γ_{av}) and S in Fig. 10 shows that both parameters decrease with the increase of S over land and ocean, which means that rain cells are gradually getting to squatty appearance as their areas increase. It is reasonable for such phenomenon physically, as the horizontal area of rain cell gets larger, there is no sufficient energy to support its overall vertical development. This is also why only a few convective systems with small areas can reach or exceed the height of the tropopause, i.e., overshooting convection (Xian and Fu, 2015). Relatively, the spatial morphology of rain cells appears taller over land than over ocean for the same S.

3.3 *The relationship between physical and geometric parameters*

Physics of rain cell generally determines its geometric nature, naturally leading to a question about relationship between rain cell physical and geometric parameters. For example, how does precipitation intensity, including convective or stratiform precipitation, of rain cells vary with their areas? How does the area fraction of convective or stratiform precipitation within rain cells change with their areas? In addition, how does the contribution of convective or stratiform precipitation to the total precipitation of rain cells change with their areas?

To answer the above questions, the relationship between RR_{max} (RR_{av}) and S for rain cells is calculated as shown in Fig. 11. Figure 11a indicates that RR_{max} of rain cells increases with the increase of S over land and

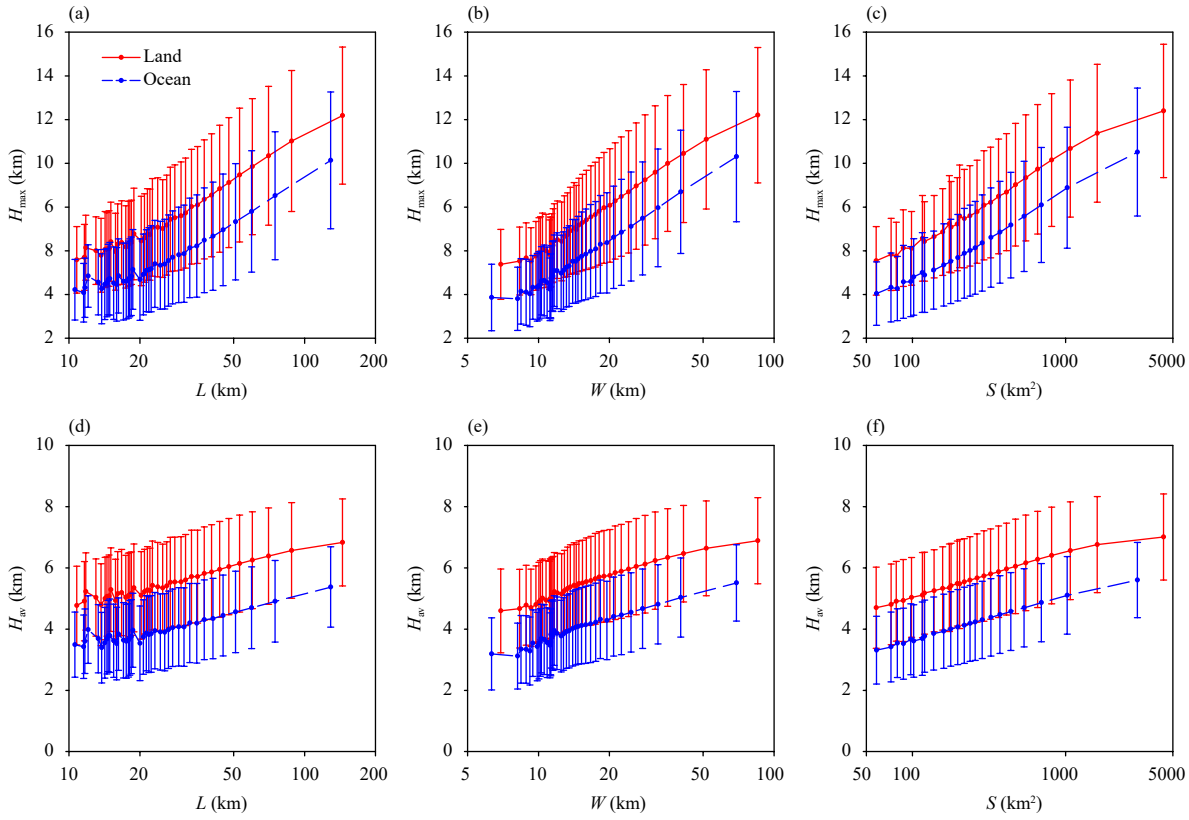

Fig. 9. Relationships between (a) H_{max} and L, (b) H_{max} and W, (c) H_{max} and S, (d) H_{av} and L, (e) H_{av} and W, and (f) H_{av} and S over tropical land and ocean from 1998 to 2012 based on the statistical principle of same samples in each interval at x axis.

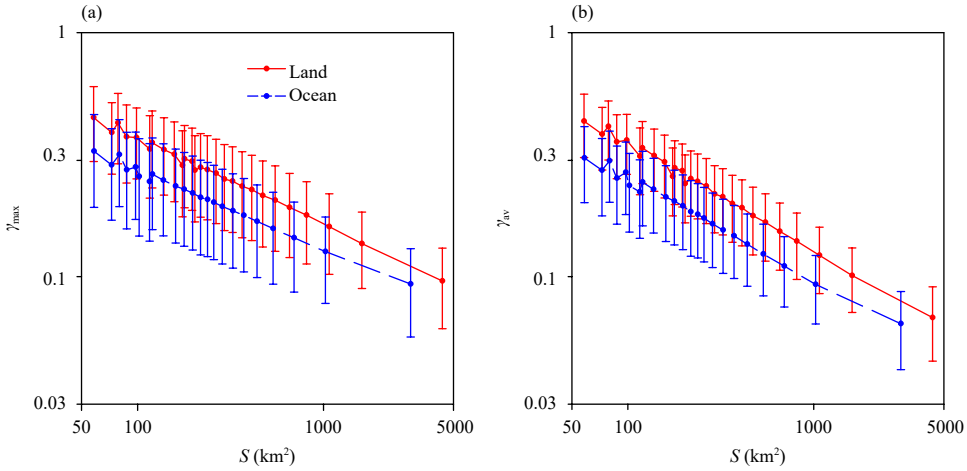

Fig. 10. Relationships between (a) γ_{max} and S, and (b) γ_{av} and S over tropical land and ocean from 1998 to 2012 based on the statistical principle of same samples in each interval at x axis.

ocean. It illustrates for this phenomenon that in the larger rain cells, there are more occurrence probability of extreme RR (RR_{max}), which may be explained as highly organization for large rain cells. Figure 11a also displays that for a given S of rain cells, RR_{max} over land is larger than that over ocean, and the difference of RR_{max} between land and ocean also increases with S, possibly because land surface may provide more energy per unit area than ocean surface.

Compared with the relationship between RR_{max} and S, the relationship between RR_{av} and S is more effective to understand how precipitation intensity affected by rain cell area. Because RR_{av} is a parameter normalized by all rain pixels within a rain cell, which reduces the influence of pixel number inequality in different rain cells. Figure 11b indicates that with the increase of S, rain cell

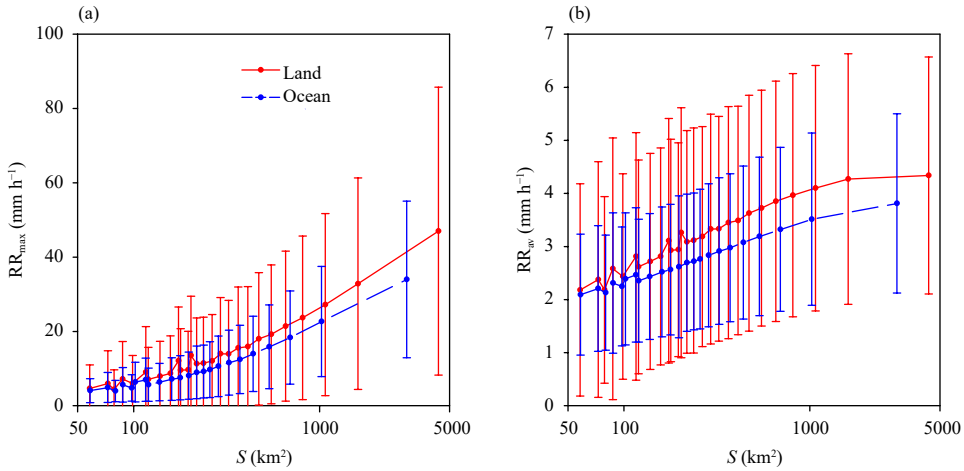

Fig. 11. Relationships between (a) RR_{max} and S, and (b) RR_{av} and S over tropical land and ocean from 1998 to 2012 based on the statistical principle of same samples in each interval at x axis.

RR_{av} increases over land and ocean, but the slope over land is greater than that over ocean. When rain cell S over land is greater than 1000 km^2, RR_{av} seems no change, keeping at 4 mm h^{-1}. The mechanism of such phenomenon is not clear now and needs to be studied in the future. While the reason that RR_{max} and RR_{av} are larger over land than over ocean for a same size rain cell, especially as rain cell S is greater than 200 km^2, is most likely more unstable atmosphere over land although wetter atmosphere over ocean.

The relationship of rain cell area S to the average rain rate and maximum rain rate of convective or stratiform precipitation, RR_{avc}, RR_{avs}, RR_{maxc}, and RR_{maxs}, is obtained as plotted in Fig. 12. Figure 12 shows that both RR_{avc} and RR_{avs} increase with the increase of S, and the same change of RR_{avc} over land and ocean, whereas the difference appears over land and ocean for RR_{avs}. For given size of rain cells, RR_{avs} over ocean is larger than that over land by 0.5 mm h^{-1}. Small RR_{avs} over land may relate to aerosols emitted by human activity (Rosenfeld et al., 2008).

Both RR_{maxc} and RR_{maxs} increase with the increase of S no matter over land and ocean. However, the increase rate of both RR_{maxc} and RR_{maxs} exceeds that of RR_{avc} and RR_{avs}, respectively. The difference of the dependence of RR_{maxc} on S between over land and ocean is also clear. When rain cell S is smaller than ~300 km^2, RR_{maxc} is slightly larger over land than that over ocean. When S increases from 300 to 5000 km^2, RR_{maxc} over land is obviously larger than that over ocean. The difference ranges from ~5 to ~10 mm h^{-1}. For RR_{maxs}, there is no clear difference over land and ocean. As S is greater than 1000 km^2, RR_{maxs} is larger over ocean than that over land. The above results indicate that heavy convective rain rate prefers to occur in large rain cells over land because of prone to instability of atmosphere over land while heavy stratiform rain rate tends to appear in large cells over ocean due to relatively stable atmosphere of ocean.

As Houze (1997) pointed out that convective (stratiform) precipitation is related to strong (weak) and young (old or decaying) convections. Therefore, the CAF (SAF) precipitation is also a proxy for the cloud evolution stage. However, except TRMM PR and GPM (Global Precipitation Measurement) DPR (Dual-frequency PR), it is difficult for passive instruments, e.g., passive microwave imagers, spectral imagers, or hyperspectral imager, to distinguish stratiform and convective precipitation. Once giving a relationship between the area fraction (or contribution of precipitation) of convective or stratiform precipitation and rain cell area, it will be possible for passive instruments to estimate the ratio of convective/stratiform precipitation in rain cells.

The relationship of the CAF/SAF within rain cell area to rain cell area S, and the relationship of the CPC/SPC within rain cell area to S, are statistically calculated as shown in Fig. 13. It displays that the area S at 800 km^2 seems to be a critical value for the variation of CAF over land and ocean. As S is less than this value, CAF increases from ~15% to ~30%, which probably corresponds to the initial development period of rain cells. Then, CAF gradually decreases as S continues to increase over land and ocean, which may mean rain cells going into decline period. Generally, the standard deviation of CAF also slightly decreases with S increase over land and ocean. The above reveals that the maximum CAF is less than 30% (20%) over land (ocean) corresponding to about 800-km^2 mean area of rain cells. It is worthy paying attention that CAF in rain cells over land

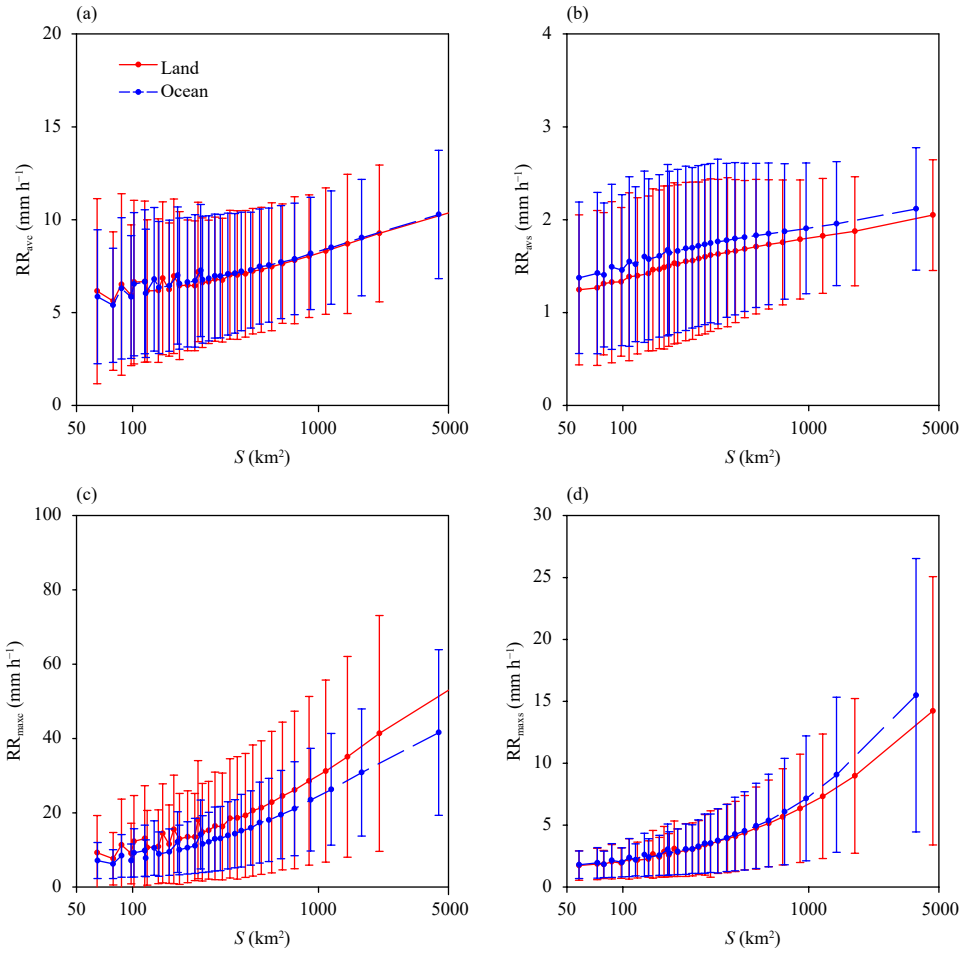

Fig. 12. Relationships between (a) RR_{avc} and S, (b) RR_{avs} and S, (c) RR_{maxc} and S, and (d) RR_{maxs} and S over tropical land and ocean from 1998 to 2012 based on the statistical principle of same samples in each interval at x axis.

is about 10% to 15% higher than that over ocean for the same size of rain cells, which may be comprehended as the result of more unstable atmospheric energy over land than over ocean.

In contrast, the relationship between SAF and S shows obvious differences from the results for CAP. Figure 13b indicates SAF increasing from 25% to 60% almost linearly with the increase of S from 50 to about 5000 km^2 over ocean, which reveals more areas of stratiform precipitation in large rain cells over ocean. However, the situation is not simple for rain cells over land. As rain cell S over land is less than 800 km^2, SAF remains at about 55%. While S increases from 800 to about 5000 km^2, SAF slightly increases from 55% to 65%. That is to say, when rain cells over land changes their size within 800 km^2, the area fraction of stratiform precipitation in rain cells remains unchanged (Fig. 13b) although the area of convective precipitation increases (Fig. 13a). When S continuously increases from 800 km^2 over land, SAF increases almost at logarithmic linear rate (Fig. 13b) contrary to CAF decrease (Fig. 13a), i.e., stratiform precipitation is the dominant rain type in large or super rain cells over land.

Combining the information in Figs. 13a, b, the sum of CAF and SAF over land stably varies from 70% to 90%, i.e., both convective and stratiform precipitation are two dominant types within rain cells over land, which is consistent with the previous studies counted by PR pixel data (Liu and Fu, 2001; Fu and Liu, 2003; Fu et al., 2008). For small rain cells over ocean, the sum of CAF and SAF is below ~60%, for large rain cells over ocean, the sum can reach to ~80%, which may suggest that there are other types of precipitation in rain cells, such as shallow precipitation and so on. Liu and Zipser (2013) found that there is almost no rain cell greater than 1000 km^2 over the regions where shallow precipitation most frequently occurs, such as Southeast Indian Ocean and Southeast Pacific. In this study, instead of mixing shallow precipitation with convective precipitation, only convective and stratiform precipitation in rain cells are statistically counted. The structure of rain cells full of shallow precipitation will be analyzed in the future.

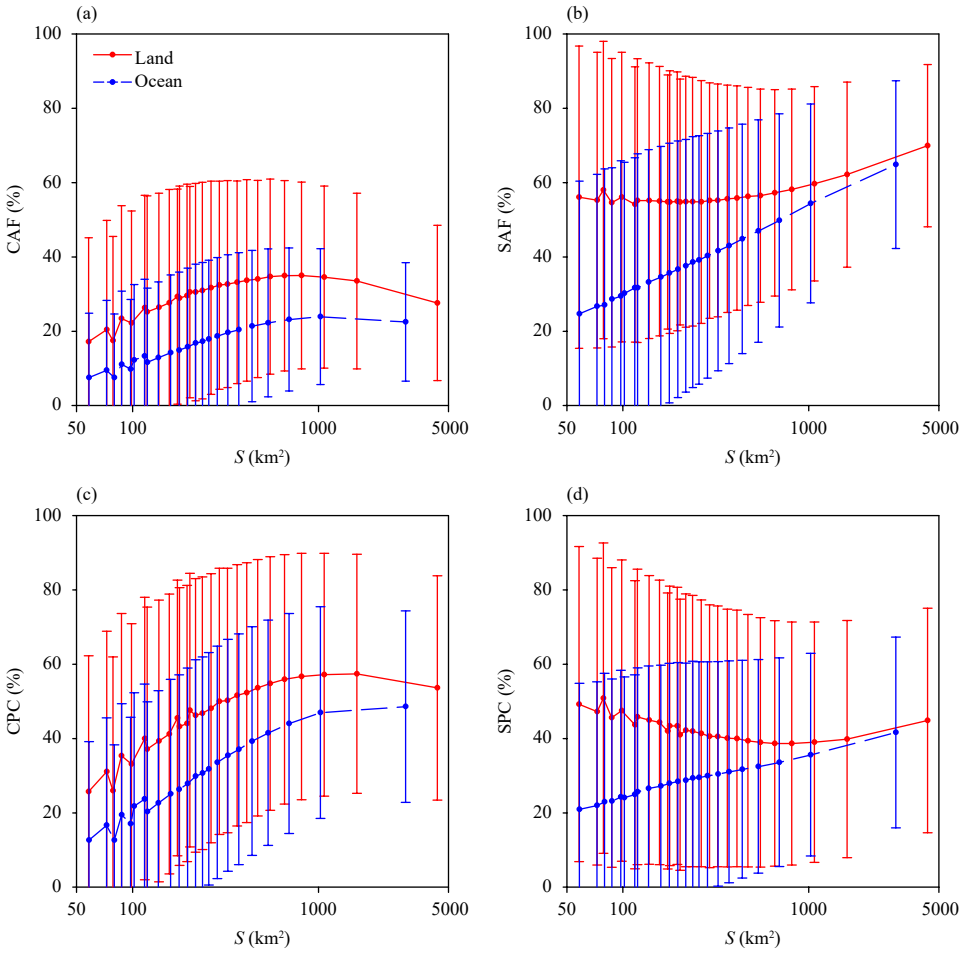

Fig. 13. Relationships between (a) CAF and *S*, (b) SAF and *S*, (c) CPC and *S*, and (d) SPC and *S* over tropical land and ocean from 1998 to 2012 based on the statistical principle of same samples in each interval at *x* axis.

The relationships between the CPC/SPC to total precipitation in rain cell and the rain cell *S* shown in Figs. 13c, d indicate the similar variation curves to Figs. 13a, b. CPC over land increases from 25% to 55% with *S* varying from 50 to 800 km^2. Then, CPC slightly decreases from 55% to 50% as *S* keeps increasing to 5000 km^2. For convective precipitation over ocean, the curve of CPC is similar to that over land but CPC is ~10% lower for a given *S*, i.e., CPC over land is about 10% higher than that over ocean for a same size rain cell because of relatively large convective precipitation intensity over land (Fig. 6). For stratiform precipitation over land, SPC decreases from 50% to 40% as *S* varies from 50 to 800 km^2. Then, it slightly increases from 40% to 45% with the increase of *S*. Over ocean, SPC simply increases from 20% to 40% with *S* at logarithmic linear rate, i.e., there are more contributions of stratiform precipitation to the total precipitation in large rain cells. Generally, the area fraction and the contribution to the total precipitation of convective precipitation in rain cells over land are 10%–15% higher than both over ocean, and high area fraction and large contribution to the total precipitation of stratiform precipitation in rain cells prefer to occur in large rain cells over land and ocean, which can be understood as there is more atmospheric unstable energy over land than over ocean, and the effect of heterogeneous topographic force on precipitation is strong over land.

3.4 *Spatial frequency distribution of rain cells in different parameters*

In order to understand the geometric and physical parameters of rain cells discussed above, the spatial distribution of rain cells corresponding to three parameters is given in this section. Situations correspond to other parameters will be introduced later articles. The first example is the spatial frequency distributions of rain cells in different α as shown in Fig. 14. Three alphas, $\alpha \leqslant 0.4$, $0.4 < \alpha \leqslant 0.7$, and $\alpha > 0.7$, are selected based on the PDF of α shown in Fig. 4c. Figure 14a indicates that rain cells

tending to the shape of long strip ($\alpha \leqslant 0.4$) appear more over the tropical ocean outside the equatorial, such as tropical Southeast and Northeast Pacific Ocean, tropical South Atlantic, and tropical southern Indian Ocean, where the frequency of this kind of rain cells is more than 14%. On the contrary, rain cells tending to be shape of square ($\alpha > 0.7$) occur more over the tropical continent (e.g., tropical Africa and tropical America) and broad Asian monsoon region, from Arabian Sea to the Bay of Bengal via Indian continent, from Indonesia to the tropical western Pacific via Indochina. The frequency of these rain cells is more than 40% (Fig. 14c). Rain cells tending to be shape between long strip and square shape ($0.4 < \alpha \leqslant 0.7$) are mainly distributed over the ocean surface, such as the tropical eastern Pacific Ocean and Atlantic Ocean on both sides of the equator, and tropical southern Indian Ocean (Fig. 14b). The frequency of such kind of rain cells in these regions is higher than 60%.

By comparing the three situations shown in Fig. 14, it is shown that the rain cell proportion of long strip shape is the smallest and that of square shape is the medium, while that of shape between long and square is the largest. This is consistent with Fig. 4c. The high frequency of square shape rain cells appearing in the tropical continents, possibly large or super-large convective cells, may be interpreted as high sensible heat forcing effect generated from land. While high frequency of rain cell shape in long strip or between long strip and square over the southeast and northeast tropical Pacific Ocean may related to the isolated and shallow convective precipitation systems. Usually, there are a lot of such kind of precipitation systems over there (Qin and Fu, 2016). However, the mechanism for most of long strip rain cells appearing over both regions needs to be further analyzed.

The second example is the spatial frequency distributions of rain cells in different γ_{av} based on its PDF shown in Fig. 5d. Figure 15a shows that rain cells in squatty appearance ($\gamma_{av} \leqslant 0.1$) are mainly located in tropical eastern Pacific, tropical South Atlantic, and tropical southern Indian Ocean, where the frequency of such rain cells exceeds 15%. It is estimated that these rain cells are shallow convective precipitation cells. Previous studies indicated that there are a lot of isolated and shallow convective clouds prevailing over these regions because of low sea surface temperature over there (Qin and Fu, 2016). Rain cells in lanky appearance ($\gamma_{av} > 0.5$, Fig. 15c) are concentrated in tropical African continent, especially tropical North African continent, where the frequency is as high as more than 12%. The western part of tropical South American continent is also high in this kind of rain

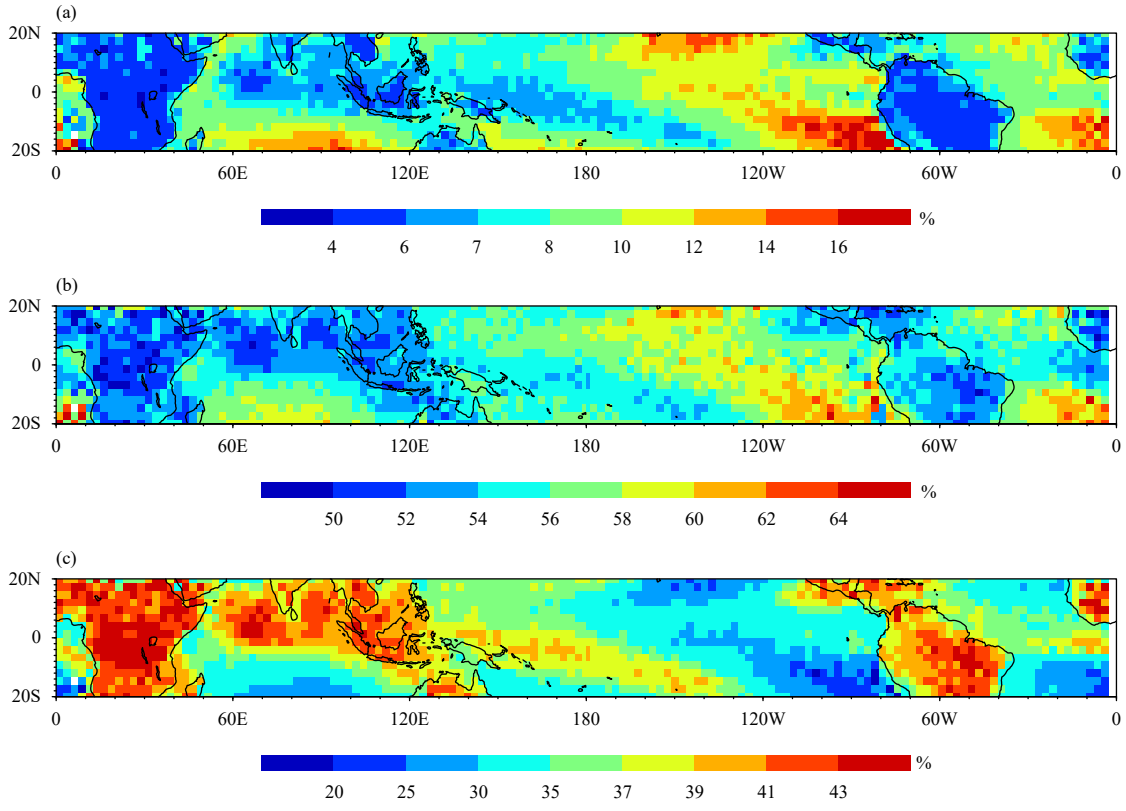

Fig. 14. Spatial frequency distributions of rain cells with (a) $\alpha \leqslant 0.4$, (b) $0.4 < \alpha \leqslant 0.7$, and (c) $\alpha > 0.7$.

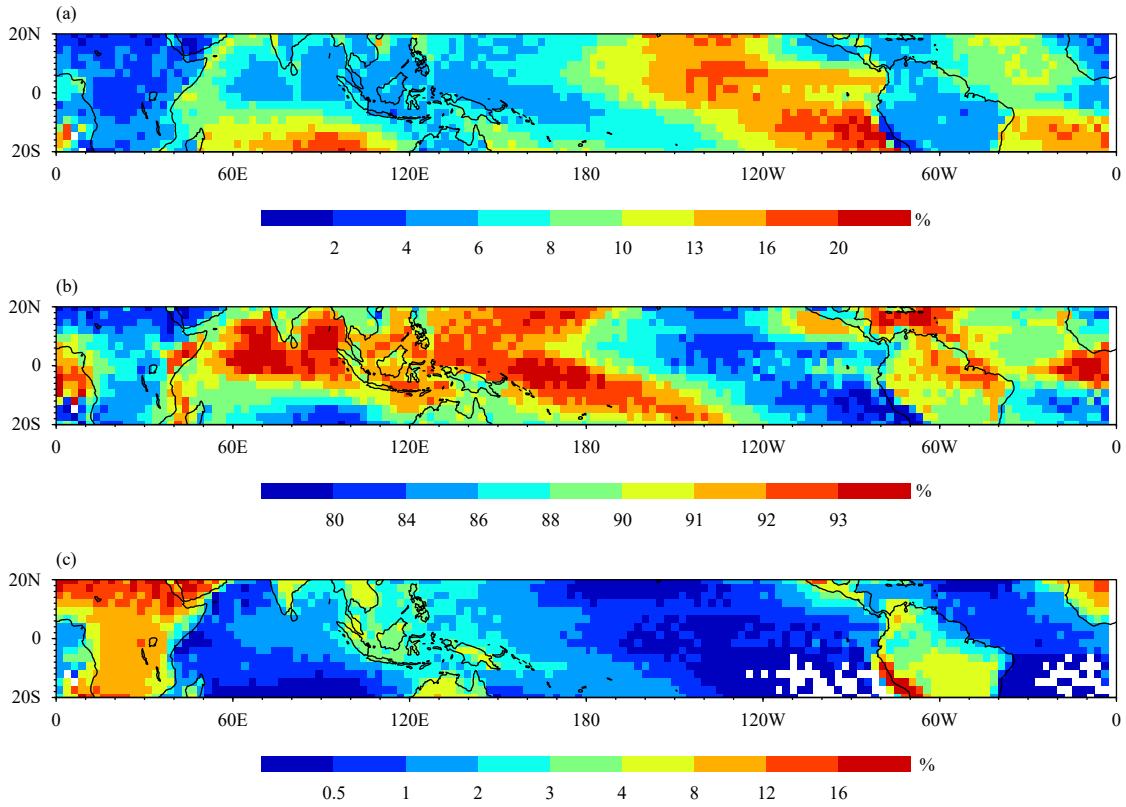

Fig. 15. Spatial frequency distributions of rain cells with (a) $\gamma_{av} \leqslant 0.1$, (b) $0.1 < \gamma_{av} \leqslant 0.5$, and (c) $\gamma_{av} > 0.5$.

cells. A wide region from northern Australia northward through Indonesia and Solomon islands to Indochina Peninsula is also a relatively high frequency (2%–8%) for this kind of rain cells. However, rain cells in lanky appearance rarely appear over ocean. Therefore, it can be speculated that these rain cells should be deep convective cells that cause the "continental chimney" in tropical Africa (Williams and Sátori, 2004; Chronis and Koshak, 2017). Figure 15b shows the highest frequency of rain cells in neither squatty nor lanky appearance ($0.1 < \gamma_{av} \leqslant 0.5$), which is consistent with that in Fig. 5d. Such rain cells are located in the broad monsoon region of Asia and the tropical western Pacific, from northern continent of South America to Caribbean, and equatorial eastern Atlantic. They represent the most widespread and common rain cells in tropics.

In the third example, the spatial frequency distributions of rain cells with different RR_{av} are shown in Fig. 16. It indicates that rain cells with light precipitation intensity ($RR_{av} \leqslant 1.5$ mm h^{-1}) are mainly located in tropical African continent, tropical eastern Pacific Ocean outside the equator and tropical western South American continent. The frequency of this kind of rain cells in these regions exceeds 35% (Fig. 16a). Rain cells with heavy rain rate ($RR_{av} > 4$ mm h^{-1}) occur mainly in equatorial Africa and its northern flank, southern Indian subcontinent, from Indonesia to Indochina Peninsula, tropical South America, and Caribbean, where the frequency of such kind of rain cells exceeds 20% (Fig. 16c). Rain cells with moderate precipitation intensity ($1.5 < RR_{av} \leqslant 4$ mm h^{-1}) are dominant proportion of rain cells in tropical oceans shown in Fig. 16b, which is consistent with Fig. 6a. They mainly appear over ocean, such as tropical southern Indian Ocean, from the equatorial Indian Ocean along Somalia to Arabian Sea, tropical central Pacific Ocean on both sides of the equator, and tropical Atlantic Ocean on both sides of the equator. The frequency in the above mentioned regions is as high as more than 70%.

From the view of probability, the comprehensive analysis in Figs. 14–16 shows that rain cells of horizontal shape in long strip (seeing Fig. 14a) over eastern Pacific Ocean outside the equator mostly are not counterpart to those of three dimensional in lanky appearances (seeing Fig. 15c), and not to those of heavy RR (seeing Fig. 16c) in these regions. While rain cells of horizontal shape in square over tropical African (seeing Fig. 14c) are not mostly those of three dimensional in squatty appearance (seeing Fig. 15a), and not to those with moderate precipitation intensity (Fig. 16b). Therefore, it is obvious that the geometric and physical parameters of rain cells

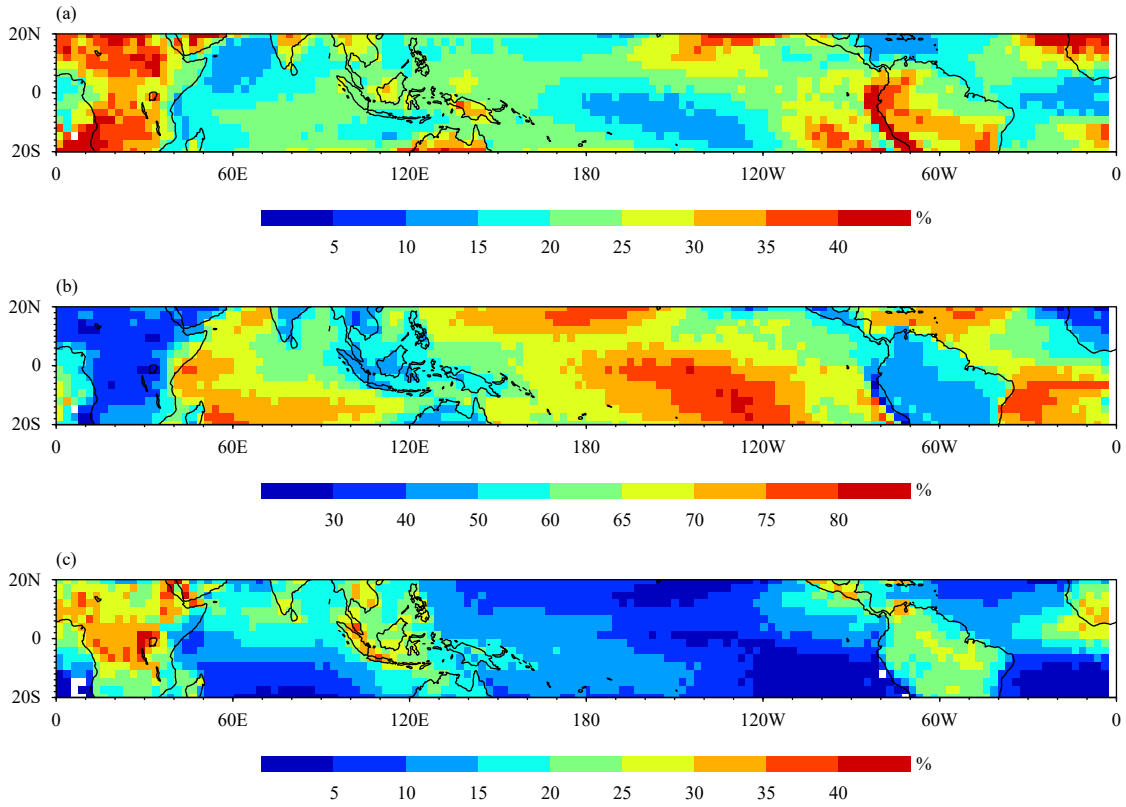

Fig. 16. Spatial frequency distributions of rain cells with (a) $RR_{av} \leqslant 1.5$ mm h^{-1}, (b) $1.5 < RR_{av} \leqslant 4$ mm h^{-1}, and (c) $RR_{av} > 4$ mm h^{-1}.

defined in this study have significance to indicate the spatial distribution characteristics and regional differences of rain cells. The details will be covered in subsequent papers.

4. Conclusions

As is known, the precipitation system controlled by associated weather systems usually consists of rain cells with different sizes. These rain cells have complex shapes as well as different properties. It is important to understand three dimensional geometric structure (i.e., geometric parameters) of rain cells together with their rainfall intensity (i.e., physical parameters) as well as the relationships among these parameters, which constitutes the most fundamental characteristics of rain cells. The knowledge on rain cells is also the basis for further study on the three dimensional structure of latent heat release from precipitation, which is important in driving the atmospheric circulation. Meanwhile, the fundamental characteristics of rain cells provide observational evidence to evaluate the numerical weather/climate models and to improve weather/climate forecast.

Compared with previous studies that directly use precipitation information based on PR pixel-level data (Liu and Fu, 2001; Fu and Liu, 2003; Fu et al., 2008, 2016), rain cells are identified through an improved approach and the MBR method, and then horizontal geometric parameters, vertical geometric parameters, and physical parameters are derived to describe their fundamental features. The method identifies more than 10^7 rain cells over the tropics detected by TRMM PR from 1998 to 2012.

The results indicate that there are about 50% of rain cells occurring at dimension of 20 km in length and 15 km in width over land and ocean. Few rain cells have the length greater than 200 km and width greater than 100 km. The possibility of horizontal appearance for rain cells in long strip or square shape is very low (less than 2%). There is an about 5% occurrence frequency for rain cell area greater than 1000 km^2. The occurrence frequency of deep rain cells over land is larger than that over ocean, the average height of rain cells varies from 2 to 10 km with peak at 5 km over land, and 2–7.5 km with peak at 3 km over ocean. The spatial morphology of rain cells shows high frequency of occurrence in lanky appearance over land while squatty appearance over ocean.

The results show a broader range of surface rainfall intensity of rain cell over land (0.4–10 mm h^{-1}) compared with that over ocean (0.4–8 mm h^{-1}). The mean RR and the maximum RR of convective and stratiform precipita-

tion show small difference between land and ocean. But the RR difference between convective and stratiform precipitation is clear. This statistical values of RR are lower than those calculated by PR pixel-level data.

Statistical results illustrate that the OFRCs decrease as the areal fraction of convective precipitation increases while such frequencies almost keep invariant when the areal fraction of stratiform precipitation varies from 10% to 80% over land and ocean. When the contribution of convective precipitation to the total precipitation increases from 15% to 90% (55%) in rain cells over land (ocean), the occurrence frequency of these cells increases. Over ocean, the OFRCs decrease as the contribution of convective precipitation to the total precipitation exceeds 55%. Usually, the OFRCs decrease as the contribution of stratiform precipitation to the total precipitation increases from 5% to 85% in rain cells over land and ocean.

Statistics shows that the shape of rain cells easily varies from square to relative long strip when their areas increase to 300 km^2. There is a log-linear relationship between the length L and width W of rain cells over land and ocean when L is longer than 20 km. Usually, for the same horizontal scale, rain cells tend to be in square shape over land while to be in line strip shape over ocean. With the increase of the horizontal scale, the horizontal structure of rain cells generally becomes looser over land and ocean. The horizontal structure of rain cells is more compact over land than over ocean while the growth of mean storm top height with the horizontal scales seems obeying a quasi-constant logarithmic linear relation. Rain cells are deeper over land than over ocean for the same horizontal scale but gradually getting to squatty shape as their areas increase.

The relationship between physical and geometric parameters of rain cells shows that the mean RR of rain cells increases with the increase of their area over land and ocean, and the increase rate over land is greater than that over ocean. When rain cell area over land is greater than 1000 km^2, the mean RR keeps at 4 mm h^{-1}. The mean RR of convective precipitation within rain cells increase with the increase of rain cell areas over land and ocean. For the same size of rain cells, the mean RR of stratiform precipitation over ocean is 0.5 mm h^{-1} larger than that over land. The results also illustrate that heavy convective rain rate prefers to occur in large rain cells over land while heavy stratiform rain rate tends to appear in large cells over ocean. Statistics also indicate that the areal fraction of convective precipitation and its contribution to the total precipitation are both higher by about 10% or 15% over land than over ocean for the same size rain cell. High areal fraction and large contribution to the total precipitation of stratiform precipitation prefer to occur in large rain cells over land and ocean.

The results also show that rain cells in long strip over eastern Pacific Ocean outside the equator are mostly not corresponding to those in lanky appearance, and not to those of heavy RR in these regions; while rain cells in square over tropical Africa are mostly not those in squatty appearance, and not to those with moderate precipitation intensity. The corresponding spatial distribution and regional differences of different rain cell parameters will be investigated in the coming studies.

Acknowledgments. The TRMM PR data can be obtained at the website https://pmm.nasa.gov/data-access/downloads/trmm.

REFERENCES

Arakawa, A., 2004: The cumulus parameterization problem: Past, present, and future. *J. Climate*, **17**, 2493–2525, doi: 10.1175/1520-0442(2004)017<2493:RATCPP>2.0.CO;2.

Austin, P. M., and R. A. Jr. Houze, 1972: Analysis of the structure of precipitation patterns in New England. *J. Appl. Meteor.*, **11**, 926–935, doi: 10.1175/1520-0450(1972)011<0926:AOTSOP>2.0.CO;2.

Awaka, J., 1989: A three-dimensional rain cell model for the study of interference due to hydrometeor scattering. *J. Commun. Res. Lab.*, **36**, 13–44.

Awaka, J., T. Iguchi, and K. Okamoto, 2009: TRMM PR standard algorithm 2A23 and its performance on bright band detection. *J. Meteor. Soc. Japan*, **87A**, 31–52, doi: 10.2151/jmsj.87A.31.

Bacchi, B., R. Ranzi, and M. Borga, 1996: Statistical characterization of spatial patterns of rainfall cells in extratropical cyclones. *J. Geophy. Res. Atmos.*, **101**, 26277–26286, doi: 10.1029/96JD01381.

Begum, S., and I. E. Otung, 2009: Rain cell size distribution inferred from rain gauge and radar data in the UK. *Radio Sci.*, **44**, RS2015, doi: 10.1029/2008RS003984.

Benjamin, S. G., and T. N. Carlson, 1986: Some effects of surface heating and topography on the regional severe storm environment. Part I: Three-dimensional simulations. *Mon. Wea. Rev.*, **114**, 307–329, doi: 10.1175/1520-0493(1986)114<0307:SEOSHA>2.0.CO;2.

Capsoni, C., F. Fedi, C. Magistroni, et al., 1987: Data and theory for a new model of the horizontal structure of rain cells for propagation applications. *Radio Sci.*, **22**, 395–404, doi: 10.1029/RS022i003p00395.

Chen, F. J., Y. F. Fu, P. Liu, et al., 2016: Seasonal variability of storm top altitudes in the tropics and subtropics observed by TRMM PR. *Atmos. Res.*, **169**, 113–126, doi: 10.1016/j.atmosres.2015.09.017.

Chen, Y. L., Y. F. Fu, T. Xian, et al., 2017: Characteristics of cloud cluster over the steep southern slopes of the Himalayas observed by CloudSat. *Int. J. Climatol.*, **37**, 4043–4052, doi: 10.1002/joc.4992.

Chronis, T., and W. J. Koshak, 2017: Diurnal variation of TRMM/LIS lightning flash radiances. *Bull. Amer. Meteor. Soc.*, **98**, 1453–1470, doi: 10.1175/BAMS-D-16-0041.1.

Dixon, M., and G. Wiener, 1993: TITAN: Thunderstorm identification, tracking, analysis, and nowcasting—A radar-based methodology. *J. Atmos. Oceanic Technol.*, **10**, 785–797, doi: 10.1175/1520-0426(1993)010<0785:TTITAA>2.0.CO;2.

Feral, L., F. Mesnard, H. Sauvageot, et al., 2000: Rain cells shape and orientation distribution in south-west of France. *Phys. Chem. Earth B: Hydrol. Oceans Atmos.*, **25**, 1073–1078, doi: 10.1016/S1464-1909(00)00155-6.

Fu, Y. F., and G. S. Liu, 2003: Precipitation characteristics in midlatitude East Asia as observed by TRMM PR and TMI. *J. Meteor. Soc. Japan*, **81**, 1353–1369, doi: 10.2151/jmsj.81.1353.

Fu, Y. F., A. M. Zhang, Y. Liu, et al., 2008: Characteristics of seasonal scale convective and stratiform precipitation in Asia based on measurements by TRMM precipitation radar. *Acta Meteor. Sinica*, **66**, 730–746, doi: 10.11676/qxxb2008.067. (in Chinese)

Fu, Y. F., A. Q. Cao, T. Y. Li, et al., 2012: Climatic characteristics of the storm top altitude for the convective and stratiform precipitation in summer Asia based on measurements of the TRMM Precipitation Radar. *Acta Meteor. Sinica*, **70**, 436–451, doi: 10.11676/qxxb2012.037. (in Chinese)

Fu, Y. F., F. J. Chen, G. S. Liu, et al., 2016: Recent trends of summer convective and stratiform precipitation in Mid-Eastern China. *Sci. Rep.*, **6**, 33044, doi: 10.1038/srep33044.

Fu, Y. F., X. Pan, T. Xian, et al., 2018: Precipitation characteristics over the steep slope of the Himalayas in rainy season observed by TRMM PR and VIRS. *Climate Dyn.*, **51**, 1971–1989, doi: 10.1007/s00382-017-3992-3.

Gagin, A., D. Rosenfeld, W. L. Woodley, et al., 1986: Results of seeding for dynamic effects on rain-cell properties in FACE-2. *J. Climate Appl. Meteor.*, **25**, 3–13, doi: 10.1175/1520-0450(1986)025<0003:ROSFDE>2.0.CO;2.

Goldhirsh, J., and B. Musiani, 1986: Rain cell size statistics derived from radar observations at Wallops Island, Virginia. *IEEE Trans. Geosci. Remote Sens.*, **GE-24**, 947–954, doi: 10.1109/TGRS.1986.289711.

Halfon, N., Z. Levin, and P. Alpert, 2009: Temporal rainfall fluctuations in Israel and their possible link to urban and air pollution effects. *Environ. Res. Lett.*, **4**, 025001, doi: 10.1088/1748-9326/4/2/025001.

Hitschfeld, W., and J. Bordan, 1954: Errors inherent in the radar measurement of rainfall at attenuating wavelengths. *J. Meteor.*, **11**, 58–67, doi: 10.1175/1520-0469(1954)011<0058:EIITRM>2.0.CO;2.

Houze, R. A. Jr., 1981: Structures of atmospheric precipitation systems: A global survey. *Radio Sci.*, **16**, 671–689, doi: 10.1029/RS016i005p00671.

Houze, R. A. Jr., 1997: Stratiform precipitation in regions of convection: A meteorological paradox? *Bull. Amer. Meteor. Soc.*, **78**, 2179–2196, doi: 10.1175/1520-0477(1997)078<2179:SPIROC>2.0.CO;2.

Houze, R. A. Jr., and A. K. Betts, 1981: Convection in GATE. *Rev. Geophys.*, **19**, 541–576, doi: 10.1029/RG019i004p00541.

Iguchi, T., T. Kozu, R. Meneghini, et al., 2000: Rain-profiling algorithm for the TRMM precipitation radar. *J. Appl. Meteor.*, **39**, 2038–2052, doi: 10.1175/1520-0450(2001)040<2038:RPAFTT>2.0.CO;2.

Johnson, R. H., S. L. Aves, P. E. Ciesielski, et al., 2005: Organization of oceanic convection during the onset of the 1998 East Asian summer monsoon. *Mon. Wea. Rev.*, **133**, 131–148, doi: 10.1175/MWR-2843.1.

Konrad, T. G., 1978: Statistical models of summer rainshowers derived from fine-scale radar observation. *J. Appl. Meteor.*, **17**, 171–188, doi: 10.1175/1520-0450(1978)017<0171:SMOSRD>2.0.CO;2.

Kummerow, C., W. Barnes, T. Kozu, et al., 1998: The Tropical Rainfall Measuring Mission (TRMM) sensor package. *J. Atmos. Oceanic Technol.*, **15**, 809–817, doi: 10.1175/1520-0426(1998)015<0809:TTRMMT>2.0.CO;2.

Kummerow, C., J. Simpson, O. Thiele, et al., 2000: The status of the Tropical Rainfall Measuring Mission (TRMM) after two years in orbit. *J. Appl. Meteor.*, **39**, 1965–1982, doi: 10.1175/1520-0450(2001)040<1965:TSOTTR>2.0.CO;2.

Lau, K. M., and H. T. Wu., 2011: Climatology and changes in tropical oceanic rainfall characteristics inferred from Tropical Rainfall Measuring Mission (TRMM) data (1998–2009). *J. Geophys. Res. Atmos.*, **116**, D17111, doi: 10.1029/2011JD015827.

Li, R., and Q. L. Min, 2010: Impacts of mineral dust on the vertical structure of precipitation. *J. Geophys. Res. Atmos.*, **115**, D09203, doi: 10.1029/2009JD011925.

Li, R., Q. L. Min, and L. C. Harrison, 2010: A case study: The indirect aerosol effects of mineral dust on warm clouds. *J. Atmos. Sci.*, **67**, 805–816, doi: 10.1175/2009JAS3235.1.

Liu, C. T., and E. Zipser, 2013: Regional variation of morphology of organized convection in the tropics and subtropics. *J. Geophys. Res. Atmos.*, **118**, 453–466, doi: 10.1029/2012JD018409.

Liu, C. T., E. J. Zipser, and S. W. Nesbitt, 2007: Global distribution of tropical deep convection: Different perspectives from TRMM infrared and radar data. *J. Climate*, **20**, 489–503, doi: 10.1175/JCLI4023.1.

Liu, G. S., and Y. F. Fu, 2001: The characteristics of tropical precipitation profiles as inferred from satellite radar measurements. *J. Meteor. Soc. Japan*, **79**, 131–143, doi: 10.2151/jmsj.79.131.

Liu, P., C. Y. Li, Y. Wang, et al., 2013: Climatic characteristics of convective and stratiform precipitation over the tropical and subtropical areas as derived from TRMM PR. *Sci. China Earth Sci.*, **56**, 375–385, doi: 10.1007/s11430-012-4474-4.

McAnelly, R. L., and W. R. Cotton, 1989: The precipitation life cycle of mesoscale convective complexes over the central United States. *Mon. Wea. Rev.*, **117**, 784–808, doi: 10.1175/1520-0493(1989)117<0784:TPLCOM>2.0.CO;2.

Nesbitt, S. W., R. Cifelli, and S. A. Rutledge, 2006: Storm morphology and rainfall characteristics of TRMM precipitation features. *Mon. Wea. Rev.*, **134**, 2702–2721, doi: 10.1175/MWR3200.1.

Pincus, R., R. Hemler, and S. A. Klein, 2006: Using stochastically generated subcolumns to represent cloud structure in a large-scale model. *Mon. Wea. Rev.*, **134**, 3644–3656, doi: 10.1175/MWR3257.1.

Qin, F., and Y. F. Fu, 2016: TRMM-observed summer warm rain over the tropical and subtropical Pacific Ocean: Characterist-

ics and regional differences. *J. Meteor. Res.*, **30**, 371–385, doi: 10.1007/s13351-016-5151-x.

Rosenfeld, D., W. L. Woodley, D. Axisa, et al., 2008: Aircraft measurements of the impacts of pollution aerosols on clouds and precipitation over the Sierra Nevada. *J. Geophys. Res. Atmos.*, **113**, D15203, doi: 10.1029/2007JD009544.

Rossow, W. B., C. Delo, and B. Cairns, 2002: Implications of the observed mesoscale variations of clouds for the Earth's radiation budget. *J. Climate*, **15**, 557–585, doi: 10.1175/1520-0442(2002)015<0557:IOTOMV>2.0.CO;2.

Sauvageot, H., F. Mesnard, and R. S. Tenório, 1999: The relation between the area-average rain rate and the rain cell size distribution parameters. *J. Atmos. Sci.*, **56**, 57–70, doi: 10.1175/1520-0469(1999)056<0057:TRBTAA>2.0.CO;2.

Schumacher, C., and R. A. Jr. Houze, 2003: Stratiform rain in the tropics as seen by the TRMM Precipitation Radar. *J. Climate*, **16**, 1739–1756, doi: 10.1175/1520-0442(2003)016<1739:SRITTA>2.0.CO;2.

Shen, D. B., G. R. North, and K. P. Bowman, 2000: A summary of reflectivity profiles from the first year of TRMM radar data. *J. Climate*, **13**, 4072–4086, doi: 10.1175/1520-0442(2000)013<4072:ASORPF>2.0.CO;2.

Short, D. A., P. A. Kucera, B. S. Ferrier, et al., 1997: Shipboard radar rainfall patterns within the TOGA COARE IFA. *Bull. Amer. Meteor. Soc.*, **78**, 2817–2836, doi: 10.1175/1520-0477(1997)078<2817:SRRPWT>2.0.CO;2.

Turk, J., and P. Bauer, 2006: The International Precipitation Working Group and its role in the improvement of quantitative precipitation measurements. *Bull. Amer. Meteor. Soc.*, **87**, 643–648, doi: 10.1175/BAMS-87-5-643.

Williams, E. R., and G. Sátori, 2004: Lightning, thermodynamic and hydrological comparison of the two tropical continental chimneys. *J. Atmos. Sol.-Terr. Phys.*, **66**, 1213–1231, doi: 10.1016/j.jastp.2004.05.015.

Xian, T., and Y. F. Fu, 2015: Characteristics of tropopause-penetrating convection determined by TRMM and COSMIC GPS radio occultation measurements. *J. Geophys. Res. Atmos.*, **120**, 7006–7024, doi: 10.1002/2014JD022633.

Tech & Copy Editor: Zhirong CHEN